EUROPEAN COMMISSION

European Research Area

Long-term Performance of Engineered Barrier Systems

PEBS

Long-term Performance of Engineered Barrier Systems

PEBS

DELIVERABLE (D-N°: D3.1-1)

Modelling and interpretation of the EB experiment hydration

DELIVERABLE (D-N°: D3.1-2)

Interpretation of the final state of the EB experiment barrier

Contract (grant agreement) number: ***FP7 249681***

Authors:

Ramon Vasconcelos, Nuria Pinyol, Eduardo Alonso, Antonio Gens (CIMNE-UPC)

Date of issue of this report: 06/06/14

Start date of project : **01/03/10** Duration : 48 Months

Project co-funded by the European Commission under the Seventh Euratom Framework Programme for Nuclear Research &Training Activities (2007-2011)		
Dissemination Level		
PU	Public	PU
RE	Restricted to a group specified by the partners of the PEBS project	
CO	Confidential, only for partners of the PEBS project	

EURATOM

TABLE OF CONTENT

List of Figures

List of Tables

1. INTRODUCTION

This report contains the main results of the coupled numerical analyses performed by CIMNE-UPC in the context of Work Package 3.1 of the PEBS Project. This Work Package focused on the Engineered Barrier Emplacement Experiment in Opalinus Clay, name usually shortened to the "EB" experiment. The aim of the experiment was to demonstrate a concept for the construction of High-Level Waste (HLW) repositories. The concept consisted in placing the canister on a bed of compacted bentonite blocks while the rest of the buffer was made of granular bentonite. More details of the test are given in the next section.

The computations have addressed both the buffer behaviour during hydration and the state of the barrier at the end of the test, as established during the dismantling operation. The coupled numerical analyses have been performed using the computer code CODE_BRIGHT (Olivella et al., 1996). As the test has been carried out under isothermal conditions, only the coupled hydromechanical formulation (HM) has been employed.

Due to the special characteristics of the granular bentonite used for most of the buffer, a double structure approach has been adopted for the description of its hydromechanical behaviour. Provision had also been made to incorporate the possibility of a variable density for the liquid phase but, in the end, it has not been required.

The PEBS proposal envisaged two separate Deliverables; D3.1-1: *Modelling and interpretation of the EB experiment hydration* and D3.1-2: *Interpretation of the final state of the EB experiment barrier.* After reviewing the work performed, it has been decided to merge the two Deliverables in this single document for a number of reasons:

- to avoid unnecessary repetitions concerning the description of the test, formulation and constitutive laws that are the same in the two situations
- to provide interested readers a single reference containing all the modelling work related to the EB experiment
- to present a more integrated view of the modelling and interpretation of the EB tests as there are no sharp distinctions between the different stages of the experiment.

The numerical simulations have been extended to longer times (100 years) but those results pertain to and are reported in Deliverable D.5-4: *Extrapolation of the models developed to the repository long-term evolution and evaluation of the uncertainties*.

After this introduction, the EB experiment is describes in Section 2 whereas Section 3 is devoted to the description of the formulation, the constitutive laws adopted and the computer code used. After presenting the main features of the numerical model in Section 4, Section 5 contains the results of the modelling concerning the hydration of the barrier and Section 6 presents the results related to the final state of the barrier. In both Sections 5 and 6, the results of the analyses are compared with the observations obtained in the experiment. The Report closes in Section 7 with a number of concluding remarks.

2. THE EB EXPERIMENT

2.1. Layout of the experiment

The engineered barrier concept under study was simulated at full scale in a niche excavated in Opalinus Clay in the Mont Terri underground laboratory in Switzerland. A detailed report of the installation is given in Mayor et al. (2005). Here only the most salient features are recorded.

The niche was horseshoe-shaped and is 15 m long, 3 m wide and 2.65 m high. A 0.97 m diameter steel cylinder simulating the canister of the Spanish reference system was emplaced on a bed of compacted Febex bentonite blocks, as shown in Figure 1. A concrete bed supported the blocks. The rest of the space between the steel cylinder and the Opalinus Clay was filled with granular bentonite made of Febex bentonite pellets placed by auger without compaction. The average density achieved was 1.38 g/cm^3 although the dry density of the pellets themselves was higher than 2.1 g/cm^3. The dry density of the blocks was 1.69 g/cm^3. The experiment was sealed with a concrete plug.

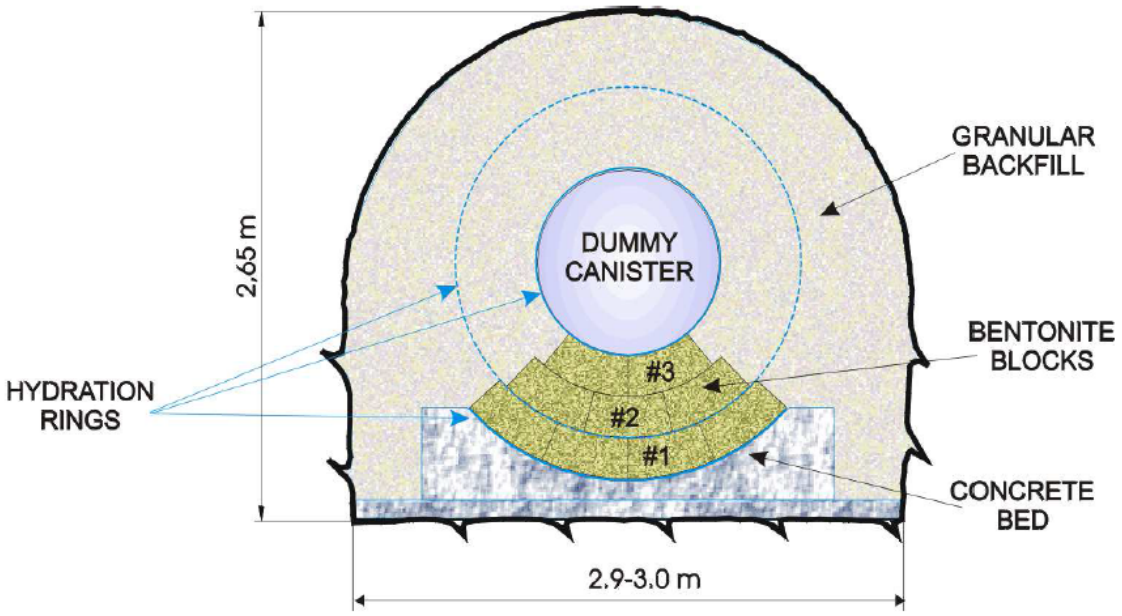

Figure 1. Layout of the EB experiment

2.2. Hydration

Because of the low permeability of the host rock (Opalinus Clay) and the desire to achieve full saturation in a reasonable period of time, artificial hydration was performed using 37 tubes placed in the granular bentonite and permeable mats located between layers of bentonite blocks. Location of tubes and mats are depicted in Figure 2 whereas Figure 3 shows a picture of the experiment during installation.

The artificial hydration history has turned out to be quite complex and it has caused difficulties to the numerical modelling due to the uncertainties associated with it. Hydration started on May 6th 2002 and Pearson water has been used throughout. Four stages can be distinguished:

- The first stage lasted two days during which water pressure was held constant and 6.7 m^3 of water entered the experiment. This high rate of hydration is due to the very high initial permeability of the granular bentonite that can be assimilated to a coarse granular material. Water was observed to exit the experiment during this phase.

- In the second stage artificial hydration was stopped for 126 days (from May 8 to September 11, 2002).
- In the third stage, artificial hydration was resumed under controlled flux conditions. This stage lasted 1741 days (from September 11, 2002 to June 18, 2007).
- In stage 4, no more water was injected into the experiment. Therefore, only natural hydration from the rock occurred in this phase that ended in the dismantling..

The evolution of the amount of injected water throughout the experiment is shown in Figure 4

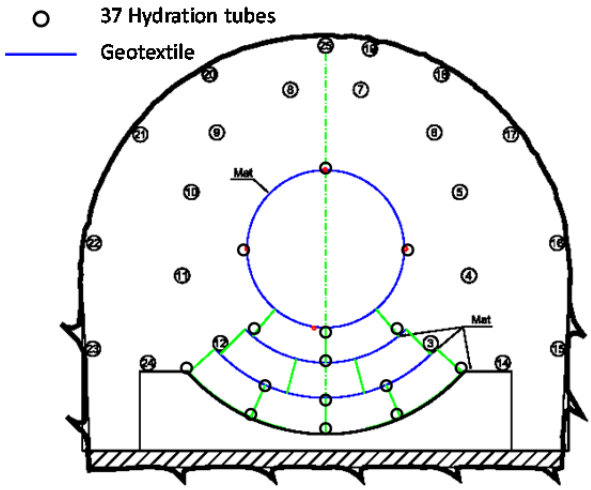

Figure 2. Layout of the artificial hydration system

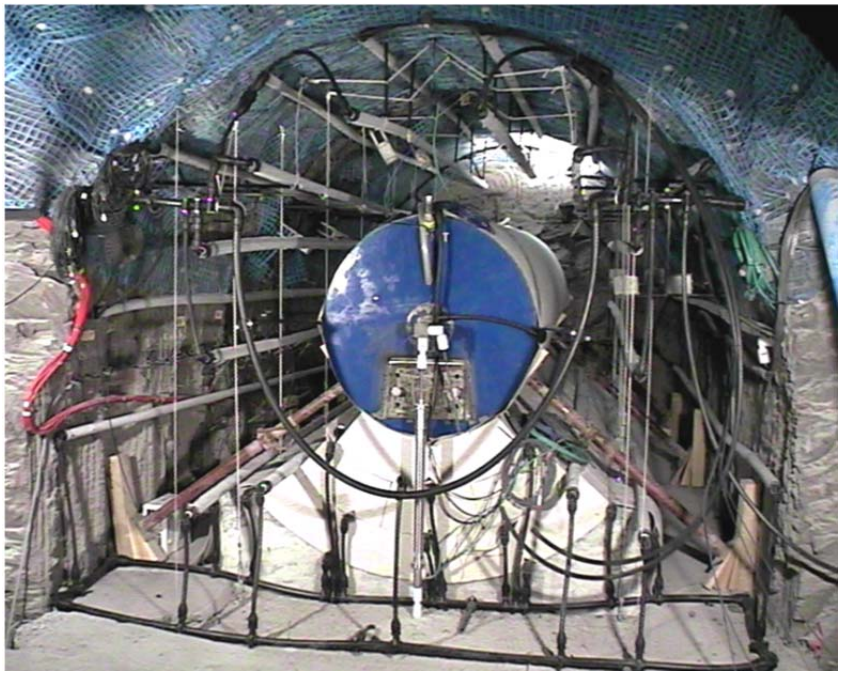

Figure 3. Installation of the EB experiment

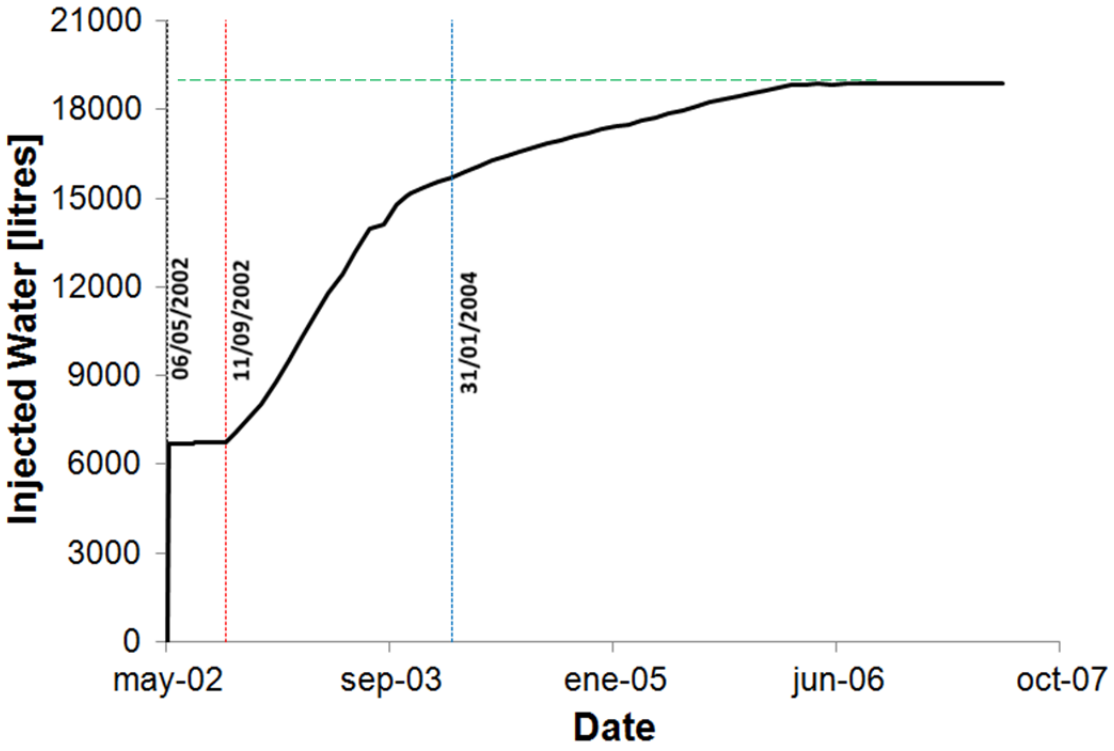

Figure 4. Evolution of injected water in the EB experiment

2.3. Instrumentation

The EB test is basically a demonstration experiment and, consequently, it is less intensively instrumented than other large scale in situ tests. In any case, relative humidity, temperatures, pore pressures, total stresses and displacements were monitored in the rock and in the bentonite barrier. In total, the measurements in the rock were performed by 20 piezometers, 8 Capacitive humidity sensors and 3 extensometers. The sensors in the bentonite buffer were 8 total stress cells, 4 extensometers (to observer cylinder displacements) and 8 capacitive humidity sensors installed in different sections along the niche. Figure 5 shows the instrumented sections and Figure 6 the location of the different sensors in the bentonite buffer. The location of some of the instrumentation placed in the rock is shown in the next two Figures, concerning relative humidity sensors (Figure 7) and pore pressure sensors (Figure 8).

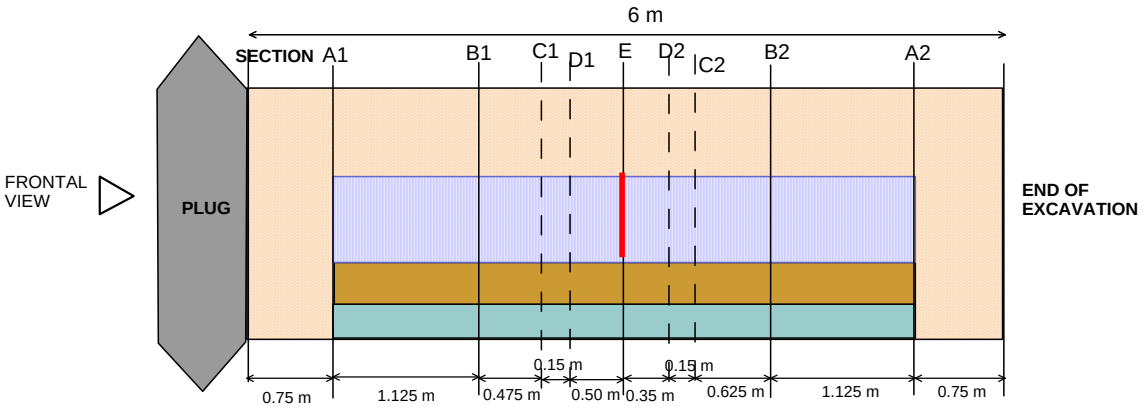

Figure 5. Instrumented sections

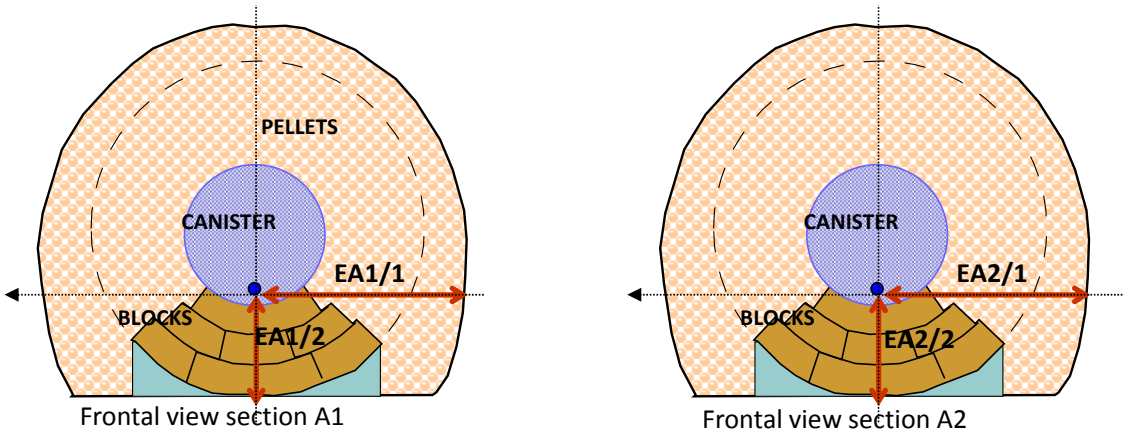

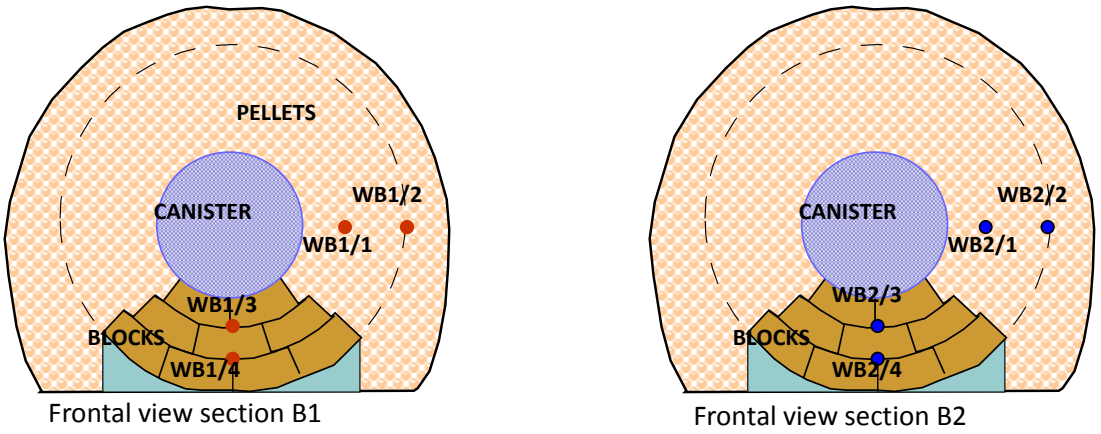

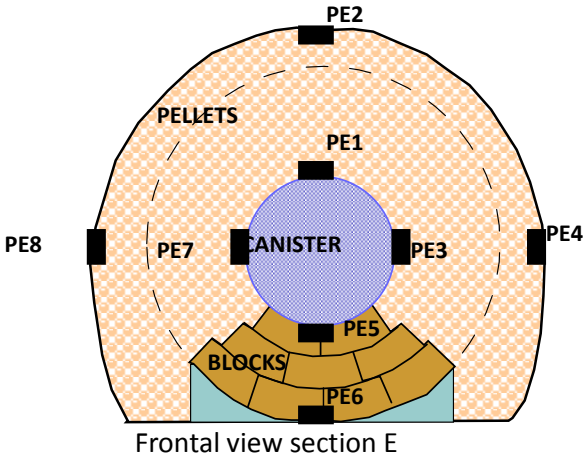

Figure 6. Location of the sensors in the buffer

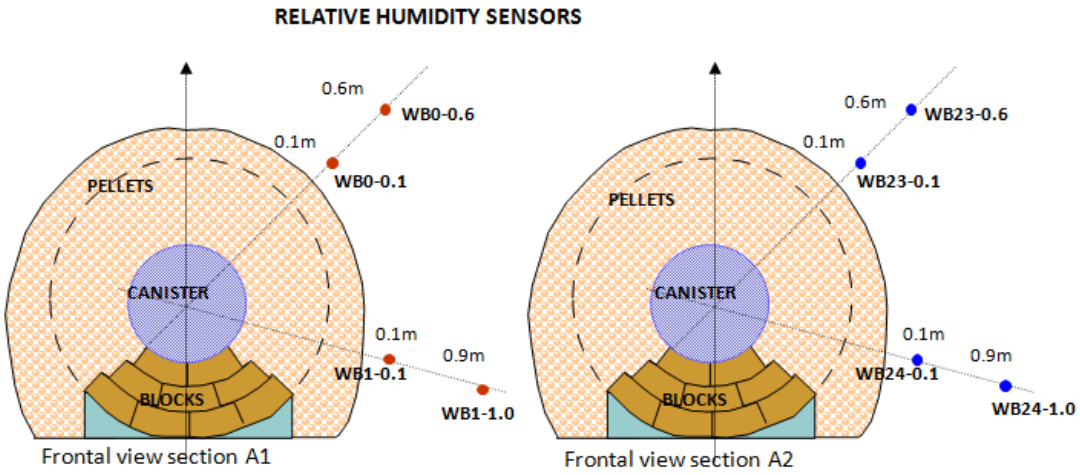

Figure 7. Relative humidity sensors installed in the Opalinus Clay

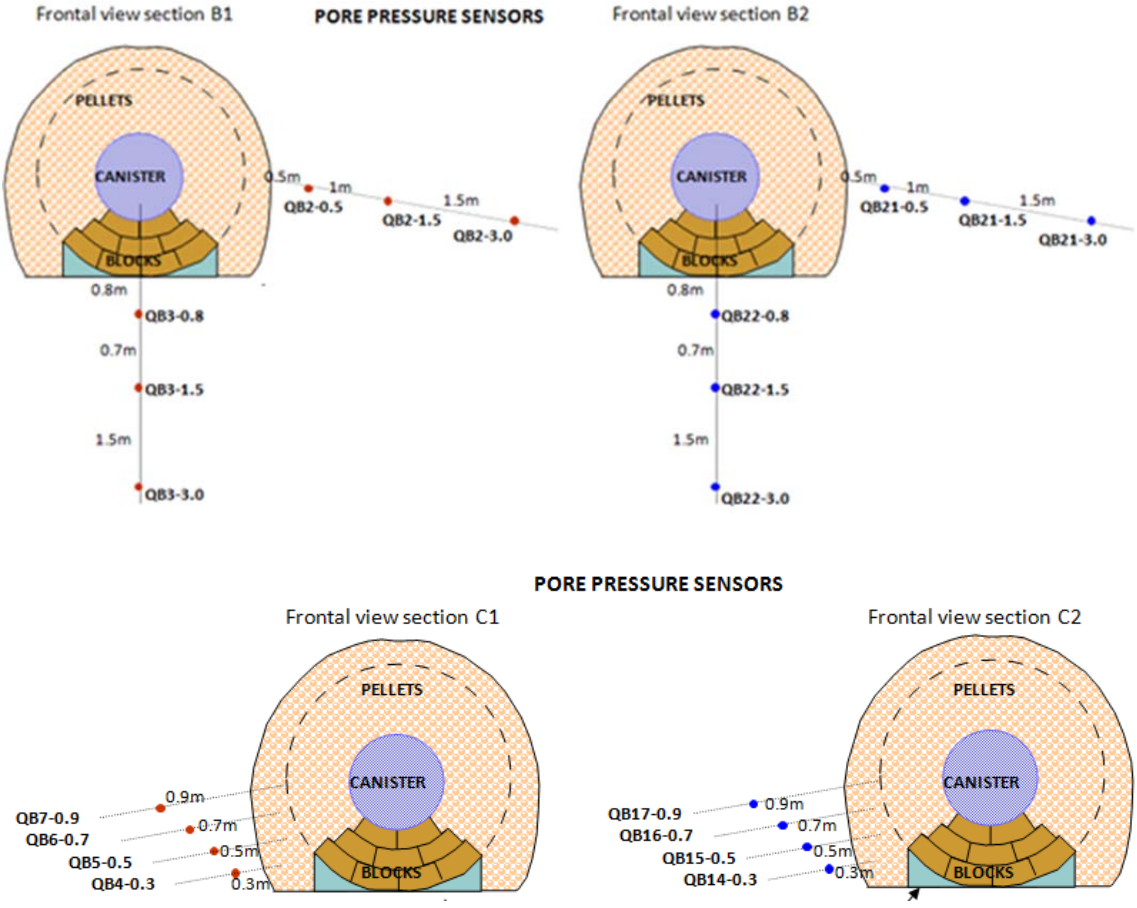

Figure 8. Pore water pressure sensors installed in the Opalinus Clay

2.4 Dismantling

After more than 10 years of operation, the EB experiment was dismantled in order to examine in detail the state of the barrier in terms of degree of saturation, density and other variables such as permeability. The dismantling operation started on October 23 2012 with a partial demolition of the plug. During the dismantling there was an intense programme of sampling carried out. Determinations of dry density and water content were performed in situ whereas block samples

were retrieved for further tests in the laboratory. Bentonite sampling started on November 23, 2012 and dismantling was declared finished on January 29, 2013.

Dismantling did not involve the steel cylinder simulating the canister that was left in place together with the concrete bed. Also, a portion of the buffer close to the rear end of the experiment was left untouched. Figure 9 shows the final state of the experiment after dismantling. Figure 10 shows a picture of the dismantled experiment. A full description of the dismantling operations and of the main results obtained is provided in Deliverable D2.1-4 (AITEMIN, 2013).

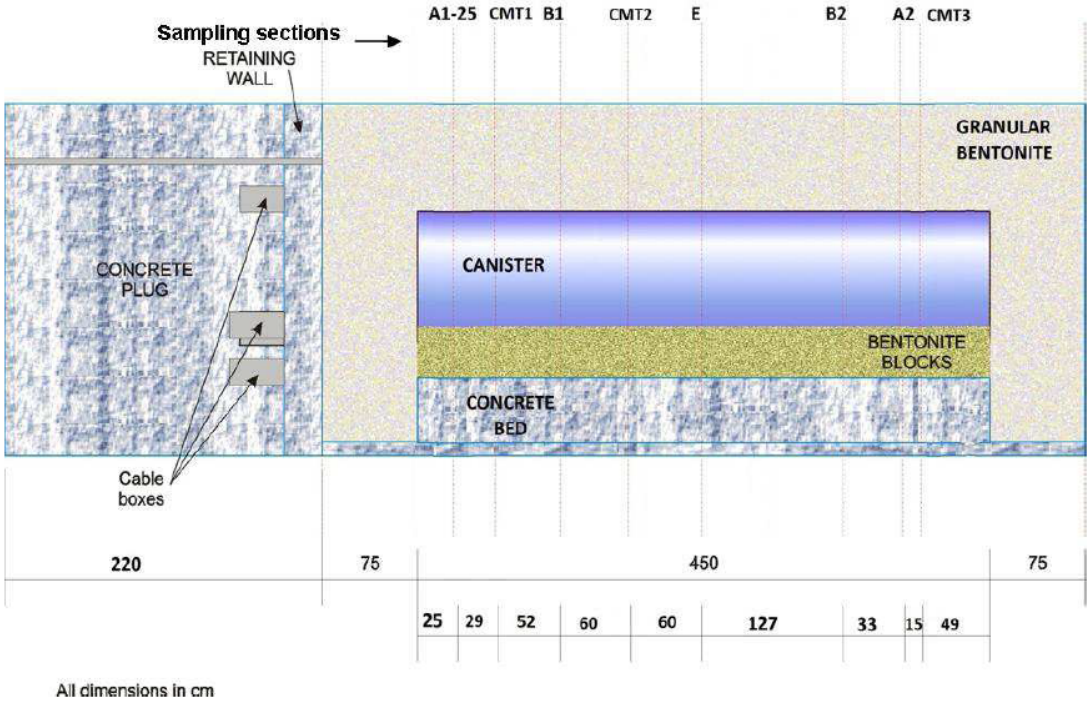

Figure 9. Final state of the EB experiment after dismantling

Figure 10. The EB experiment after dismantling

3. FORMULATION, CONSTITUTIVE EQUATIONS AND COMPUTER CODE

3.1 Formulation

The formulation is a reduced version of that presented in Deliverable 3.5.2 (Gens & Sanchez 2014) from which the thermal aspects have been removed. Thus the basic set equations to be considered are the balances of water, gas, solid and momentum (equilibrium).

3.1.1 *Balance of mass of water:*

$$\frac{\partial}{\partial t}\left(\theta_l^w S_l \phi + \theta_g^w S_g \phi\right) + \nabla.\left(\mathbf{j}_l^w + \mathbf{j}_g^w\right) = f^w \tag{1}$$

where θ_l^w and θ_g^w are the masses of water per unit volume of liquid and gas phase respectively. ϕ is the porosity and S_α is the volumetric fraction of pore volume occupied by the alpha phase (α=*l,g*). $\mathbf{j}_l^w$ and $\mathbf{j}_g^w$ denote the total mass fluxes of water in the liquid and gas phases with respect to a fixed reference system. f^w is the external mass supply of water per unit volume of medium.

3.1.2 *Balance of mass of air:*

$$\frac{\partial}{\partial t}\left(\theta_l^a S_l \phi + \theta_g^a S_g \phi\right) + \nabla.\left(\mathbf{j}_l^a + \mathbf{j}_g^a\right) = f^a \tag{1}$$

where θ_l^a and θ_g^a are the masses of air per unit volume of liquid and gas phase respectively. $\mathbf{j}_l^a$ and $\mathbf{j}_g^a$ denote the total mass fluxes of air in the liquid and gas phases with respect to a fixed reference system. f^a is the external mass supply of air per unit volume of medium. Note that dry air is considered as a single species in spite of the fact that it is a mixture of gasses. The gaseous phase is assumed as a mixture of air and water vapour. Air is also dissolved in the liquid phase.

3.1.3 *Balance of mass of solid:*

$$\frac{\partial}{\partial t}\left(\rho_s\left(1-\phi\right)\right) + \nabla\cdot\left(\rho_s\left(1-\phi\right)\dot{\mathbf{u}}\right) = 0 \tag{3}$$

where $\dot{\mathbf{u}}$ is the solid velocity vector. The variation of porosities in terms of changes in solid density and volumetric deformation of the soil skeleton is obtained from (3).

3.1.4 *Balance of momentum (equilibrium):*

$$\nabla.\boldsymbol{\sigma}_t + \mathbf{b} = 0 \tag{4}$$

where $\boldsymbol{\sigma}_t$ is the total stress tensor and $\mathbf{b}$ the vector of body forces. In (4) inertial terms have been neglected. This assumption is usually accepted because both velocities and accelerations are small, yielding terms that are negligible in comparison with the stress terms. The assumption of small strain rate is also made. Through an adequate constitutive model, the equilibrium equation is transformed into a form expressed in terms of the solid velocities, fluid pressures and temperatures.

3.2 Constitutive equations

Naturally, no thermal constitutive equations are considered in this case. Also some phenomena such as vapour transport are neglected because of the isothermal conditions.

3.2.1 *Mechanical*

The mechanical response of the compacted bentonite blocks is described by means of a thermo-elastoplastic model proposed by Alonso et al. (1990), commonly known as the Barcelona Basic Model (BBM). Changes in the volumetric component of the elastic strain are computed by the incremental expression

$$d\varepsilon_v^{el} = \frac{\kappa_i}{(1+e)}\frac{dp}{p} + \frac{\kappa_s}{(1+e)(s+p_{atm})}ds \tag{5}$$

where κ_i and κ_s are parameters related to the volumetric compressibility against changes in net mean stress and suction, respectively; e is the void ratio and p_{atm}, the atmospheric pressure. The dependence of compressibility parameters on suction and stress level are expressed by

$$\kappa_i(s) = \kappa_{i0}(1+\alpha_i s) \tag{6}$$

and

$$\kappa_s(p,s) = \kappa_{s0}\left[1+\alpha_{sp}\ln\left(\frac{p}{p_{ref}}\right)\right]\cdot e^{\alpha_{ss}s} \tag{7}$$

κ_{i0} and κ_{s0} are the initial (zero suction) elastic slope for specific volume-mean stress and for specific volume-suction relationships, respectively; α_I, α_{sp}, α_{ss}, are model parameters. A form of the classical Modified Cam-Clay model is taken as the reference yield surface:

$$F^{LC} = J^2 - \frac{M^2}{3}(p+p_s)(p_0-p) = 0 \tag{8}$$

where J is the second invariant of the deviatoric stress tensor and M is the limiting critical state slope, which is assumed to be constant. p_o, p_s are considered dependent on suction:

$$p_0 = p^c\left(\frac{p_0^*}{p^c}\right)^{\frac{\lambda(0)-\kappa_{i0}}{\lambda(s)-\kappa_i(s)}} \tag{9}$$

$$p_s = -k\cdot s \tag{10}$$

where

$$\lambda(s) = \lambda(0)\cdot\left(r+(1-r)e^{-\beta s}\right) \tag{11}$$

p_0* represents the saturated preconsolidation stress; $\lambda(s)$ is the slope of the virgin compression curve at suction s; p^c is a reference stress; k controls the increase in the tensile strength with suction; r, β control the rate of increase of soil stiffness with suction. Hardening depends on plastic volumetric strain according to

$$\frac{dp_0^*}{p_0^*} = \frac{1+e}{\lambda(0)-\kappa_{i0}} d\varepsilon_{vol}^p \tag{12}$$

A general view of the yield surface shape in *p*-*q*-*s* space and the more remarkable features of BBM as the loading-collapse (LC) yield curve are shown in Figure 11. A detailed explanation of the mathematical formulation, capabilities and limitations of this strain-hardening model can be found in Alonso et al. (1990).

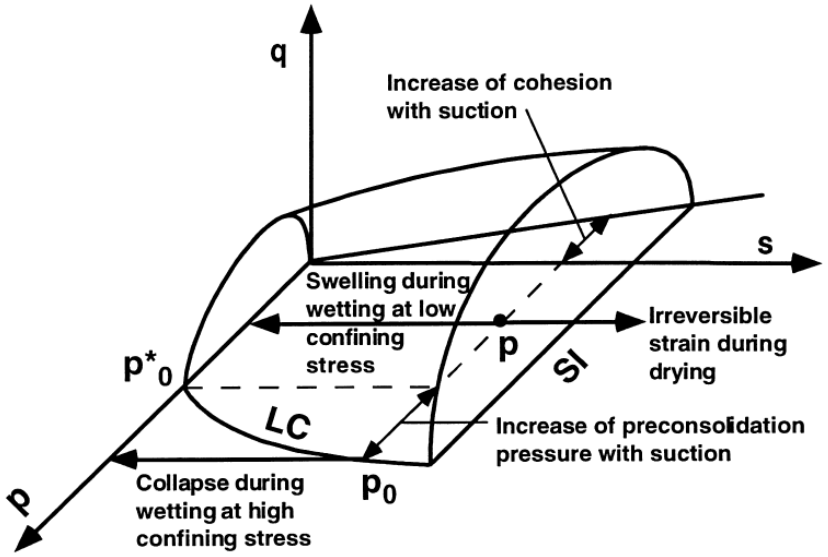

Figure 11. BBM yield surface in *p*-*q*-*s* space

On the other hand, the hydro-mechanical response of pellets during the hydration test is performed through a double porosity approach considering the decomposition of total deformation into a contribution provided by the micro level associated to its highly clay activity and another one arising from the macro level (that corresponds to the strain between aggregates) as it can be seen in the following equation:

$$d\varepsilon_{kl} = d_{kl}^{Macro} + d\varepsilon_{kl}^{micro} \tag{13}$$

The macrostructural behaviour can be described by equations for unsaturated non-expansive soils such as the ones presented previously. The microstructural behaviour is controlled by physical-chemical phenomena at clay particle level. It is assumed that microstructure is saturated and its deformation is reversible, volumetric and independent of macrostructural effects. The stress-strain relationship is established through the following expressions:

$$d\sigma_{ij} = D_{ijkl}^{Macro}\left(d\varepsilon_{kl}^{Macro} - \delta_{kl}\frac{ds^{Macro}}{3K_s^{Macro}} - d\varepsilon_{kl}^{LC} - d\varepsilon_{kl}^{SD} - d\varepsilon_{kl}^{SI} \right) \tag{14}$$

$$d\sigma_{ij} = D_{ijkl}^{micro}\left(d\varepsilon_{kl}^{micro} - \delta_{kl}\frac{ds^{micro}}{3K_s^{micro}} \right) \tag{15}$$

where D_{ijkl}^{Macro} , D_{ijkl}^{micro} are the mechanical elastic matrix of the clay which relates stress and elastic deformation at macro ($d\varepsilon_{kl}^{Macro}$) and micro ($d\varepsilon_{kl}^{micro}$) levels, respectively; K_s^{Macro}, K_s^{micro} are the bulk moduli against macro and micro suction changes (if any), respectively; $d\varepsilon_{kl}^{LC}$ are the macro plastic strains of the clay if LC (loading-collapse curve) is activated; $d\varepsilon_{kl}^{SD}$ and $d\varepsilon_{kl}^{SI}$

are the macro plastic strains of clay if SD (Suction Decrease) and SI (Suction Increase) yield surfaces are activated, respectively. Mechanical elastic matrices are defined by clay bulk moduli against net stress changes (K^{Macro} and K^{micro} at macro and micro levels, respectively) and clay Poisson's ratio ($\nu^{Macro} = \nu^{micro}$). These bulk moduli are considered to be linearly dependent of the logarithmic mean stress by

$$K^{Macro} = \frac{\left(1 + e^{Macro}\right)p}{\kappa^{Macro}} \tag{16}$$

$$K^{micro} = \frac{\left(1 + e^{micro}\right)\left(p + s^{micro}\right)}{\kappa^{micro}} \tag{17}$$

where e^{Macro} and e^{micro} are the macro and micro void ratio, respectively; κ^{Macro} and κ^{micro}, the elastic stiffness at macro and micro levels, respectively, for changes in mean stress. An effective stress concept generalized for unsaturated conditions (the term $p+s^{micro}$ in equation (17)) describes the behaviour of microstructure. Bulk modulus against suction changes, K_s^{Macro}, is assumed to be linearly dependent of the logarithmic suction through the expression

$$K_s^{Macro} = \frac{\left(1 + e\right)\left(s^{Macro} + p_{atm}\right)}{\kappa_s^{Macro}} \tag{18}$$

The two last terms in Equation (14) compute the interaction between micro and macro structures. Coupling between these two structural levels takes into account irreversible macrostructural strains when elastic microstructural strains take place. In other words, microstructural swelling induces irreversible increase of the macro void ratio while microstructural shrinkage leads to a decrease of that property. Furthermore irreversible macrostructural deformations induced by microstructural swelling/shrinkage are assumed to be proportional to elastic microstructural strains according to interaction functions (Gens & Alonso, 1992; Alonso et al., 1999; Sánchez et al., 2005). A general expression for the plastic volumetric strain induced by microstructural strain (in its incremental form), $d\varepsilon_{vol}^{m \to M}$, is given by

$$d\varepsilon_{vol}^{m \to M} = f \cdot d\varepsilon_{vol}^{micro} = d\varepsilon_{vol}^{SD} + d\varepsilon_{vol}^{SI} \tag{19}$$

where f represents the coupling function between the micro and macro levels. Two interaction functions are defined: f^{SD} for SD paths and f^{SI} for SI paths. These micro-macro coupling functions are dependent on the degree of openness of the macrostructure relative to the applied stress state (evaluated by the ratio p/p_0) according to

$$f^{SD} = f_{SD0} + f_{SD1}\left(1 - \frac{p}{p_0}\right)^{n_{SD}} \tag{20}$$

$$f^{SI} = f_{SI0} + f_{SI1}\left(\frac{p}{p_0}\right)^{n_{SI}} \tag{21}$$

in which f_{SD1}, n_{SD} are parameters for the micro-macro coupling function when SD is activated while f_{SI1}, n_{SI} are the corresponding parameters when SI is activated. A general shape for these coupling functions is shown in Figure 12.

The hardening law for the double-structure formulation considers the dependency of the saturated isotropic yield locus on the total plastic strain (arising from the activation of the LC curve and/or the micro-macro coupling) through

$$\frac{dp_0^*}{p_0^*} = \frac{\left(1+e^{Macro}\right)}{\lambda-\kappa}\left(d\varepsilon_{vol}^{LC} + d\varepsilon_{vol}^{SD} + d\varepsilon_{vol}^{SI}\right) \tag{22}$$

while the evolution of history micro-macro coupling variables (when SD or SI is activated) is described by means of the following hardening law:

$$d\gamma^{\alpha} = \frac{K^{micro}}{f^{SD}} d\varepsilon_{vol}^{SD} + \frac{K^{micro}}{f^{SI}} d\varepsilon_{vol}^{SI} \tag{23}$$

where the index "α" stands for the plastic mechanism (SD or SI) that activates irreversible deformation in the macro level.

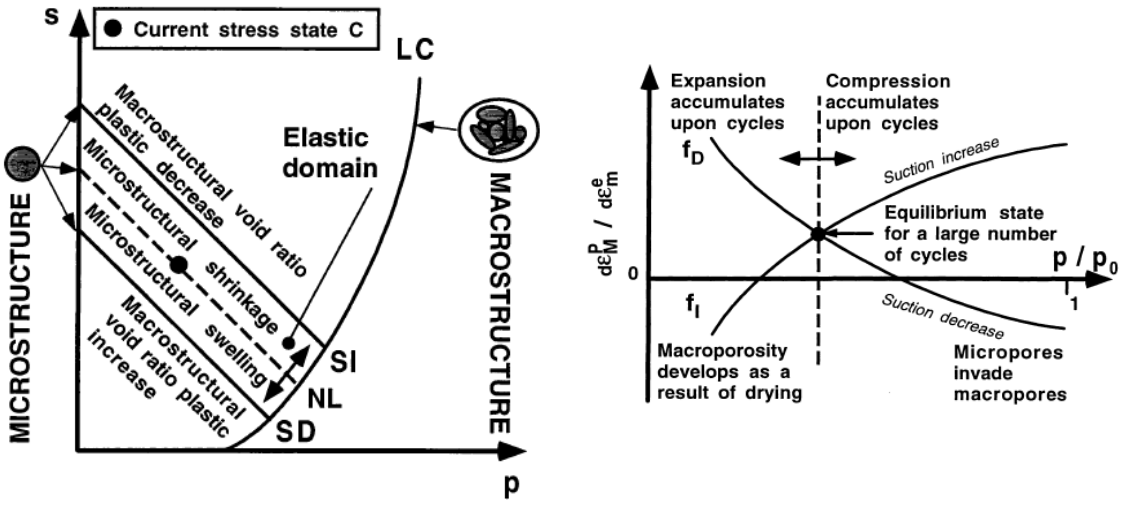

(a) (b)

Figure 12. Main features of the double porosity constitutive model (a) yield surface in *p*-*s* plane, (b) micro-macro level interaction functions and mechanisms.

3.2.2 *Hydraulic*

Because gas pressure is considered constant ion the analyses, only the advctrive flow of liquid is considered. It is computed using generalized Darcy's law, expressed as:

$$\mathbf{q}_l = -\mathbf{K}_l\left(\nabla P_l - \rho_l \mathbf{g}\right); \tag{24}$$

where P_l is the liquid pressure, $\mathbf{K}_l$ is the permeability tensor and $\mathbf{g}$ is the gravity vector. The permeability tensor is not constant and depends on other variables, according to:

$$\mathbf{K}_l = \mathbf{k}\frac{k_{rl}}{\mu_l}; \tag{25}$$

where **k** is the intrinsic permeability tensor, μ_l is the liquid dynamic viscosity and k_{rl} is the liquid relative permeability. The dependence of intrinsic permeability on pore structure is considered in terms of total porosity according to:

$$\mathbf{k} = k_0 \frac{\phi^3}{(1-\phi)^2} \frac{(1-\phi_0)^2}{\phi_0^3} \mathbf{I} \tag{26}$$

where k_0 is the reference permeability at the reference porosity ϕ_0.

The relative permeability of the liquid phase (k_{rl}) is made dependent on the degree of saturation according to:

$$k_{rl} = S_{el}^{\ n} \tag{27}$$

where n is a model parameter and S_{el} the effective degree of saturation, evaluated as follows:

$$S_{el} = \frac{S_l - S_{lr}}{S_{ls} - S_{lr}} \tag{28}$$

where S_{lr} is the residual saturation and S_{ls} is the maximum saturation.

The retention curve adopted in the conventional formulation is based on the one proposed by van Genuchten (1978). The relation between degree of saturation and suction is given by:

$$S_{el} = \left[1 + \left(\frac{s}{P_o} \right)^{\frac{1}{1-\lambda_o}} \right]^{-\lambda_o} f_d \tag{29}$$

where P_o and λ_o are model parameters and f_d is a function included in order to model properly the high suction range where. The adopted expression is the following:

$$f_d = \left(1 - \frac{s}{P_d} \right)^{\lambda_d} \tag{30}$$

where P_d is related with the suction at 0 degree of saturation and λ_d is a model parameter. When $\lambda_d = 0$ the original model is recovered (Gens et al., 1998).

When the double porosity model is used, it is possible to track the values of the macroporosity and the microporosity at every stage of the hydration of the barrier. The effect of microfabric evolution on liquid flow is taken into account by assuming that the flow of liquid water takes place only through the macropores. Consequently, the intrinsic permeability is a function of the macro porosity through the exponential law:

$$\mathbf{k} = k_0 \exp[b(\phi_M - \phi_{M0})]\mathbf{I} \tag{31}$$

where k_0 is the intrinsic permeability at the reference macroporosity ϕ_{M0}, ϕ_M is the macroporosity, b is a model parameter and **I** is the identity matrix.

3.3 Computer code and numerical implementation

The analyses presented in this report have been performed by the computer code CODE_BRIGHT (Olivella et al., 1996; CODE_BRIGHT User's Manual, 2014), a finite element code designed to solve thermo-hydro-mechanical problems in geological media. One unknown (state variable) is associated with each of the balance equations presented. The unknowns are obtained by solving the system of balance equations numerically in a coupled way.

The state variables are: solid velocity, **u** (one, two or three spatial directions); liquid pressure, P_l and gas pressure, P_g. From state variables, dependent variables are calculated using the constitutive equations or the equilibrium restrictions. Strains are defined in terms of displacements. Small strains and small strain rates are assumed for solid deformation. Advective terms due to solid displacement are neglected after the formulation is transformed in terms of material derivatives (in fact, material derivatives are approximated as eulerian time derivatives). The numerical approach can be viewed as divided in two parts: spatial and temporal discretization. Galerkin finite element method is used for the spatial discretization while finite differences are used for the temporal discretization. The discretization in time is linear and an implicit scheme is used. Finally, since the problem presented here is non-linear, the Newton-Raphson method was adopted as iterative scheme.

4. FEATURES OF THE ANALYSES

4.1 Geometry, initial conditions and boundary conditions

A 2-D plane strain mesh was adopted to represent the modelled domain. The domain is 80 m wide and 80 m high. Taking advantage of symmetry, only one half of the problem was simulated. Furthermore the initial stress state in the rock was assumed to be anisotropic with vertical and horizontal stress values of 6.0 and 4.8 MPa, respectively. A constant value of 1.0 MPa was assumed for the initial water pressure in the host rock. These values reproduce quite well the initial conditions in the EB experiment site before the tunnel opening (Alonso & Hoffman, 2007). The external mechanical boundary conditions were 0-displacement on the vertical and the lower horizontal boundaries. A compressive vertical stress of 6.0 MPa was applied on the upper horizontal boundary. A liquid pressure of 1.0 MPa was prescribed along the upper and lower horizontal boundaries and on the right vertical boundary of the modelled domain. The modelled geometry and the initial and boundary conditions prior to the excavation are given in **Error! Reference source not found.**Figure 13

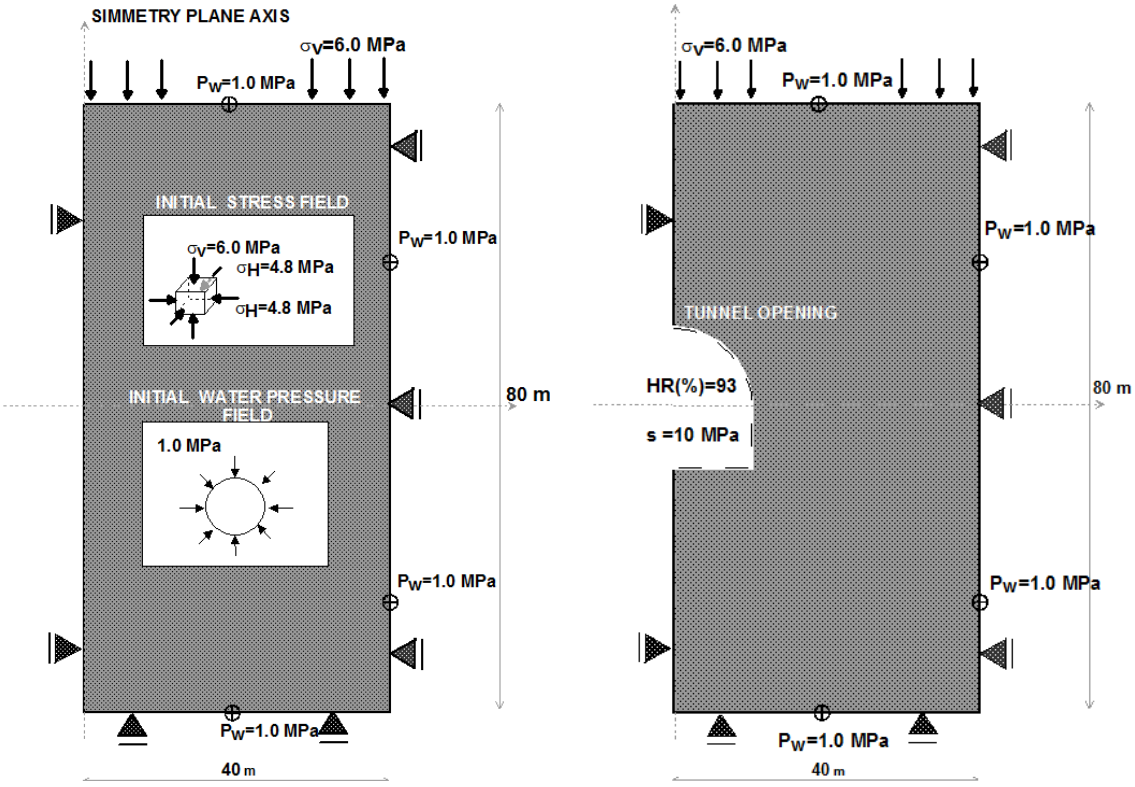

Figure 13. Geometry, initial and boundary conditions before tunnel excavation (left) and after tunnel excavation (right)

4.2 Tunnel excavation and buffer emplacement

The tunnel was excavated 160 days before the emplacement of the buffer materials. The excavation was modelled by a relaxation of the total stresses. A constant suction of 10.0 MPa was imposed on the tunnel surface that corresponds to a relative humidity of about 93%. The excavated damage zone around the tunnel was considered through a modelled material with the same hydro-mechanical properties of the rock formation (Opalinus Clay) except for its initial porosity, water permeability and air entry suction. EDZ has a width of 5.0 m. Figure 13 shows the geometry of the excavation and the boundary conditions for the tunnel construction. The horse-shoe shape of the actual tunnel has been reproduced.

Once the tunnel has been constructed, the buffer materials were emplaced. At this stage the rounded concrete base to hold the bed of "FEBEX" bentonite blocks was first constructed, then the bentonite blocks and the cylinder (simulating the canister) were emplaced, the instrumentation system was installed, the hydration system was set up, the retaining wall was constructed and then, granular bentonite (pellets) were emplaced. The numerical modelling was simplified in such a way that only the central portion of the EB experiment was taken in account, the emplacement of all buffer materials was made instantaneously and the hydration tubes were simulated by 34 injection points distributed over the whole cross section. The geotextile material around the cylinder, between adjacent compacted block layers and in the interface between the concrete basis and the clay blocks was also modelled through very thin lines of finite elements. The initial stress and water pressure fields in the host rock correspond to the end of the excavation period. The initial suction for the bentonite pellets and compacted blocks was set to 300 MPa and 150 MPa, respectively. The initial stress state for the bentonite based materials was assumed to be isotropic with a confining stress of 0.3 MPa. Figure 14 shows a detailed view of the buffer materials distribution inside the EB niche site. A period of time of 5 days was left before the hydration phase starts.

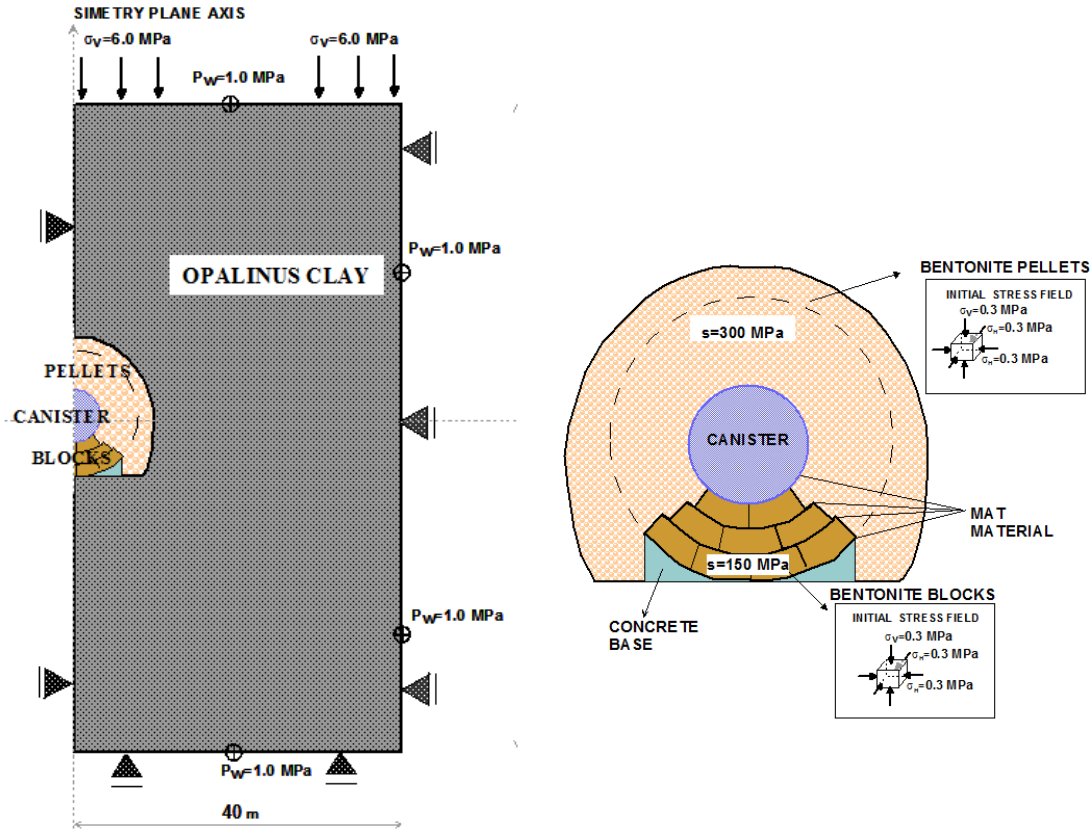

Figure 14. View of the clay barrier emplacement, distribution of materials and their initial state inside the barrier

4.3 Hydration boundary conditions

In order to reproduce the hydration experiment in a satisfactory way the wetting history was divided into four main phases:

- The first phase involved the injection of 6.7 m^3 of water during the first two days. A flux boundary condition of 0.033 m^3/day was applied in each injection point per meter of the experiment section.

- The second phase of hydration refers to a period of 126 days of natural water redistribution when no water was injected. No water inflow through the injection points was prescribed.

- In the third phase of hydration, water was injected again. At this stage a water injection pressure was applied at every injection point according to the injection pressure evolution shown in Figure 15 (black continuous line) that reproduces approximately the observed water injection pressure variation. This phase covers a period of 1741 days (from September 11, 2002 to June 18, 2007). It can be noted that from July 31, 2006 to June 18, 2007 a constant liquid pressure of 20 kPa was prescribed at every injection point.

- In the fourth phase of hydration, no further water was injected into the bentonite buffer, all injection valves were closed on after June 18, 2007. Again, no water inflow through the injection points was prescribed.

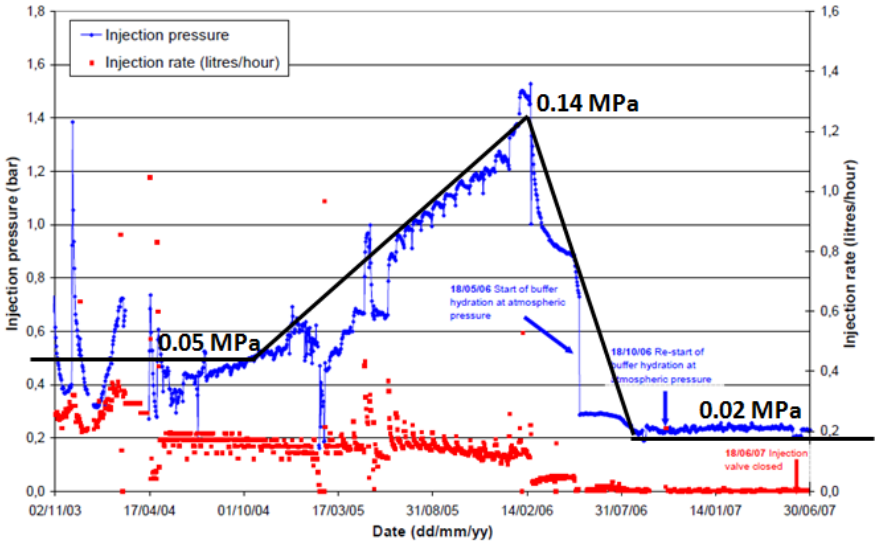

Figure 15. Injection rate and injection pressure from the start of artificial hydration (AITEMIN, 2013). The hydraulic boundary conditions is represented by the black continuous line

4.4 Model parameters

Parameters required for the double-structure model were calibrated from the numerical modelling of wetting-drying tests at constant vertical load and wetting at constant volume carried out by Hoffman (2005) on bentonite pellet mixtures with dry density values between 1.30 and 1.90 Mg/m^3. Laws and parameters used for the compacted bentonite blocks were taken from previous studies performed during the FEBEX project (ENRESA, 2000). Parameters for the host rock (Opalinus Clay) were taken from the updated dataset provided by the HE-E Experiment (HE-E Experiment 2013). The water content-suction relationships for the buffer materials are given in Figure 16. The retention curve for the pellets was taken from the experimental data provided by Hoffman et al. (2007) for samples with dry density of 1.30 Mg/m^3 (somewhat different form the average dry density of granular mixtures in the EB experiment reported to be about 1.36 Mg/m^3).

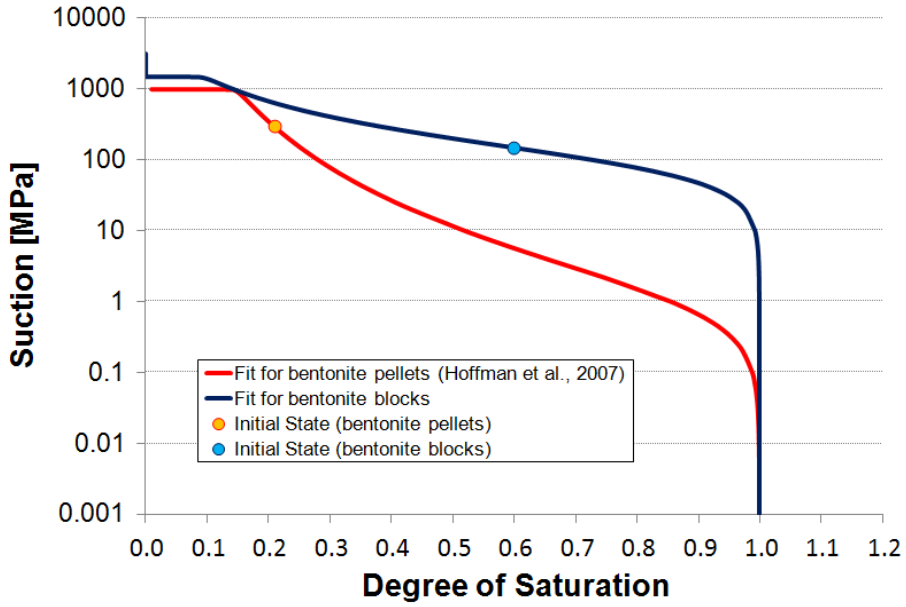

Figure 16. Water retention curves for the bentonite pellets (red line) and for the bentonite blocks (blue line)

Water permeability may play a crucial role during hydration of clay barriers. Due to the high swelling potential of bentonite pellets, these granular materials tend to exhibit a decrease in porosity when wetted, and consequently a reduction in liquid permeability even by several orders of magnitude. The dependence of the intrinsic permeability (**k**) on porosity (ϕ) is considered in the numerical modelling through the Kozeny expression

$$\mathbf{k} = \mathbf{k_0} \frac{\phi^3}{(1-\phi)^2} \frac{(1-\phi_0)^2}{\phi_0^3} \tag{32}$$

where $\mathbf{k}_o$ is the intrinsic permeability at a reference porosity, ϕ_0. When the double-porosity conceptual approach is used for modelling the constitutive response of a material, macroporosity is the input variable in equation (32). Experimental data from several infiltration tests on pellet samples allowed the calibration of the (exponential) dependence of water permeability on their saturation state (Hoffman et al., 2007). The hydro-mechanical properties used in the numerical calculations are summarized in Tables 1 to 6..

Table 1. Physical properties

Physical Properties	**Opalinus Clay (Intact rock)**	**Opalinus Clay (EDZ)**	**Granular Bentonite**	**Bentonite Blocks**
Solid grain density [kg/m^3]	2640	2640	2700	2700
Porosity	0.12	0.14	0.496	0.37

Table 2. Hydraulic parameters

Hydraulic Parameters	Opalinus Clay (Intact rock)	Opalinus Clay (EDZ)	Granular Bentonite	Bentonite Blocks
Retention Curve[a]				
P_0 [MPa]	18.0	9.00	0.95	100
σ_0 [N/m]	7.20e-02	7.20e-02	7.20e-02	7.20e-02
λ''	0.400	0.400	0.217	0.450
P_d [MPa]	1.0e27	1.0e27	1.00e03	1.50e03
λ_d	0	0	0.02	0.05
$S_{rw} - S_{ws}$	0.01– 1.00	0.01 – 1.00	0.01 – 1.00	0 – 1.00
Liquid Permeability [b]				
Intrinsic Permeab.	1.00e-20	5.00e-20	1.00e-16	1.10e-21
Initial Porosity, ϕ_0	0.12	0.14	0.20	0.37
Shape Parameter,	1.00	1.00	1.00	1.00
Shape Parameter,	3.00	3.00	1.90	3.00

[a] Parameter for the Modified Van Genuchten model : $S_e = \left[1+\left(\frac{P_a - P_w}{P}\right)^{\frac{1}{1-\lambda''}}\right]^{-\lambda''} \cdot \left(1-\frac{P_a - P_w}{P_d}\right)^{\lambda_d}$.

[b] Parameter for the Relative Permeability Law: $k_{rw} = A \cdot S_e^{\lambda'}$

Table3. Mechanical parameters for Opalinus Clay (Elastic Constitutive Law)

	Young Modulus [MPa]	Poisson's Ratio
Opalinus Clay (Intact rock)	3000	0.30
Opalinus Clay (EDZ)	3000	0.30

Table 4. Mechanical parameters for compacted blocks (Barcelona Basic Model)

Mechanical Parameters	**Bentonite Blocks**
TEP Elastic Parameters	
κ_{i0}	0.02
κ_{s0}	0.052
Minimum bulk moduli, [MPa]	4.50
Poisson's ratio, ν	0.20
Parameter for expansive material, α_{ss}	-0.007
Parameter for expansive material, α_i	-0.003
Parameter for expansive material, α_{sp}	-0.12
TEP Plastic Parameters	
λ(0)	0.180
r	0.75
β [MPa^{-1}]	0.05
k	0.10
p_{s0} [MPa]	0.10
p^c [MPa]	0.100
M	1.50
e_0	0.590
p_0* [MPa]	14.0

Table 5. Mechanical parameters for the pellets (Barcelona Expansive Model)

Mechanical Parameters	**Bentonite Pellets**
Elastic Behaviour	
κ_{macro} [MPa]	0.02
κ_{micro} [MPa]	0.02
$\kappa_{s\ macro}$ [MPa]	0.0001
Poisson's ratio, ν_m	0.44
Minimum bulk modulus at macro level,	0.0001
Minimum bulk modulus at micro level, $K_{min,,micro}$ [MPa]	0.0001
Elastoplastic Behaviour (BBM in p-q diagram)	
Slope of the virgin loading line in the e-ln(p) diagram, λ(0)	0.20
Coefficient setting the change in cohesion with suction, r	0.65
Coefficient setting the change in cohesion with suction, β [MPa^{-1}]	0.01
Reference pressure, p^c [MPa]	0.075

	Coefficient setting the increase of tensile strength with suction , k_s	0.0
	Cohesion for suction equal to zero, p_{t0} [MPa]	0.100
	Slope of the critical line, M	1.30
Coupling Behaviour		
	Parameter micro-macro when SD is actived, f_{sd1}	1.30
	Parameter micro-macro when SD is actived, n_{sd}	5.00
	Parameter micro-macro when SI is actived, f_{si1}	2.00
	Parameter micro-macro when SI is actived, n_{si}	0.10

Table 6. Hydraulic and mechanical parameters for the concrete bed, geotextile and cylinder

		Concrete	**Geotextile**	**Cylinder**
Retention Curve Parameters	P_0 [MPa]	100	10	1000
	σ_0 [N/m]	7.20e-02	7.20e-02	7.20e-02
	λ''	0.33	0.60	0.33
	P_d [MPa]	1.0e27	1.0e27	1.0e27
	λ_d	0	0	0
	$S_{rw} - S_{ws}$	0.001– 1.00	0.01 – 1.00	0.001 – 1.00
Water Permeability Parameters	k_0 [m^2]	1.00e-19	1.00e-14	1.00e-40
	ϕ_0	0.07	0.50	0.01
	Shape par., A	1.00	1.00	1.00
	Shape par., λ'	8.00	2.00	8.00
	$S_{rw} - S_{ws}$	0.001– 1.00	0.01 – 1.00	0.001 – 1.00
Elastic Model Parameters	E [MPa]	3.00e05	6.00e03	2.10e05
	ν	0.30	0.30	0.30

5. RESULTS OF THE HYDRATION PHASE

5.1 Evolution of relative humidity

The evolution of the relative humidity was monitored in the clay barrier (sections B1 and B2) and in the first meter into the Opalinus Clay (sections A1 and A2) during the hydration phase. Data provided by relative humidity sensors served as an indication of the progress of hydration. To compute suction values, the psychometric (Kelvin's) equation has been used. It relates relative humidity (RH) and total suction (ψ) through

$$\Psi = -\frac{\rho_w RT}{M_w} \ln(RH) \tag{33}$$

where ρ_w is the water density, R is the universal gas constant, T is the absolute temperature and M_w is the molecular mass of water. A total of four RH sensors were emplaced in each of mentioned sections. Observed and computed values of relative humidity and suction are presented in Figures 17 and 18 for the buffer and the rock respectively.

The evolution of the relative humidity inside the clay barrier (Figure 17) indicates a fast reduction in suction (that corresponds to a quick increase in RH) after the first phase of hydration, where a volume of about 6.7 m^3 of water was injected in only two days. This can be noted especially in those sensors located inside the compacted blocks (sensors WB13 and WB14 in section B1 and WB23 and WB24 in section B2). For the sensors located inside the pellets, it can be observed that the rate of resaturation is lower for those ones in section B2 but this section is completely saturated 450 days after the beginning of the hydration experiment while the period of time required for the full resaturation of section B1 seems to be longer than 850 days. The bentonite blocks reach a saturated condition at the same time for both instrumented sections. The rock volume close to the excavated tunnel is almost saturated during the hydration phase (see Figure 18). The desaturation induced by the ventilation period in the tunnel (about 160 days) prior to the emplacement and hydration of the EB is also detected by the monitoring system.

Concerning the computed results (full lines in the Figures), significant discrepancies can be observed between model computations and the experimental data, especially concerning the hydration of the pellets. The fast resaturation of the clay barrier predicted by the model may be a consequence of the relative large volume of water initially injected in calculations. In fact, reported water losses through the host rock and the concrete plug were not measured which implies that the real amount of water inside of the clay barrier after the first phase of hydration is unknown and probably quite lower than the applied 6.7 m^3 of injected water for this phase. In the case of bentonite blocks, model predictions in RH seem to agree better with the experimental data.

Considering the sensors in the part of rock close to the top of the tunnel and near the rock-pellets interface (sensor WB0_01 in section A1 and WB23_01 in section A2), it was observed a similar episode of desaturation followed by a fast resaturation (between days 150 and 450 of the hydration period). Although this event was not well predicted by the model, numerical results for the sensors closer to the tunnel (sensors WB0_01 and WB1_01 in section A1 and WB23_01 and WB24_01 in section A2) show a similar response characterized by a small reduction of RH (due to excavation effects and to the water taken from the rock during the first stages of resaturation of the clay barrier) followed by a complete resaturation of these zones once the pellets are almost saturated.

5.2 Evolution of pore water pressure

Pore pressure evolution in the near field of the experiment was monitored by means of 12 sensors in four boreholes (3 sensors in each borehole) installed in sections B1 and B2 (see Figures 19 and 20) and of 8 additional sensors emplaced in individual boreholes in sections C1 and C2, four sensors per section (see Figure 21). Measured and computed values for the pore water pressure show a good agreement and reinforce the almost saturated condition of the host rock as discussed in the previous section. The drainage effect of the tunnel excavation (prior to the hydration experiment), the decrease in liquid pressure due to the flow of water towards the clay barrier in the early stages of the experiment and the tendency towards recovering the pore pressure to values above the atmospheric pressure as the barrier becomes saturated can be observed in the numerical results.

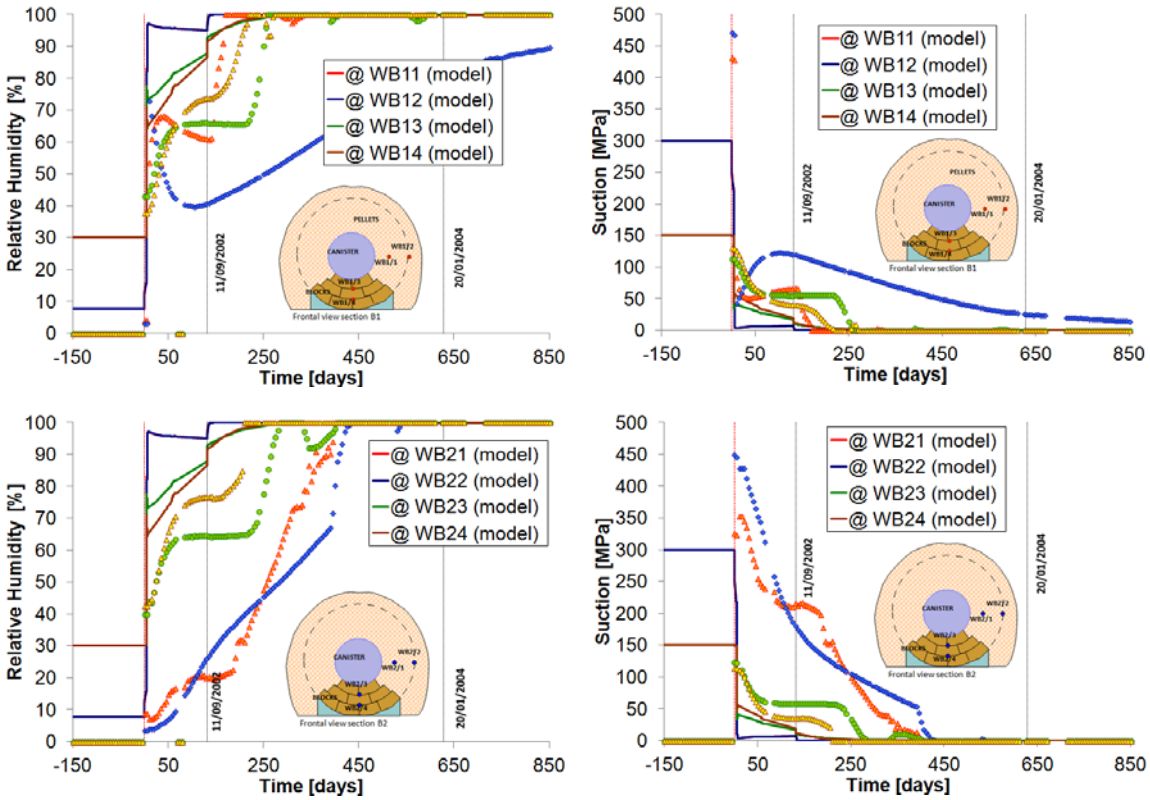

Figure 17. Evolution of relative humidity (left) and suction (right) inside the buffer material for sensors in the instrumented sections B1 (up) and B2 (down). Model predictions are denoted by full lines while symbols represent the experimental data

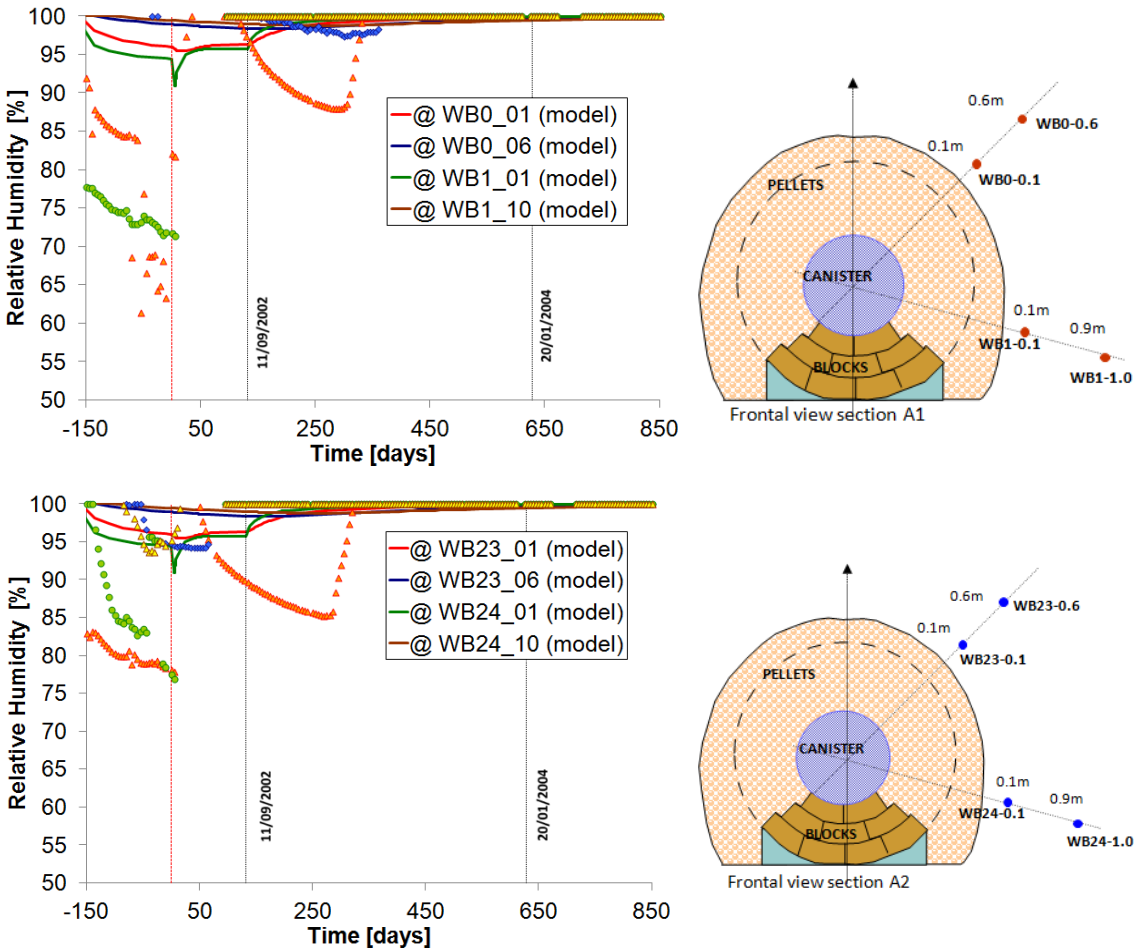

Figure 18. Computed and measured relative humidity in the rock for sensors in the instrumented sections A1 (up) and A2 (down). Model predictions are denoted by full lines while symbols represent the experimental data

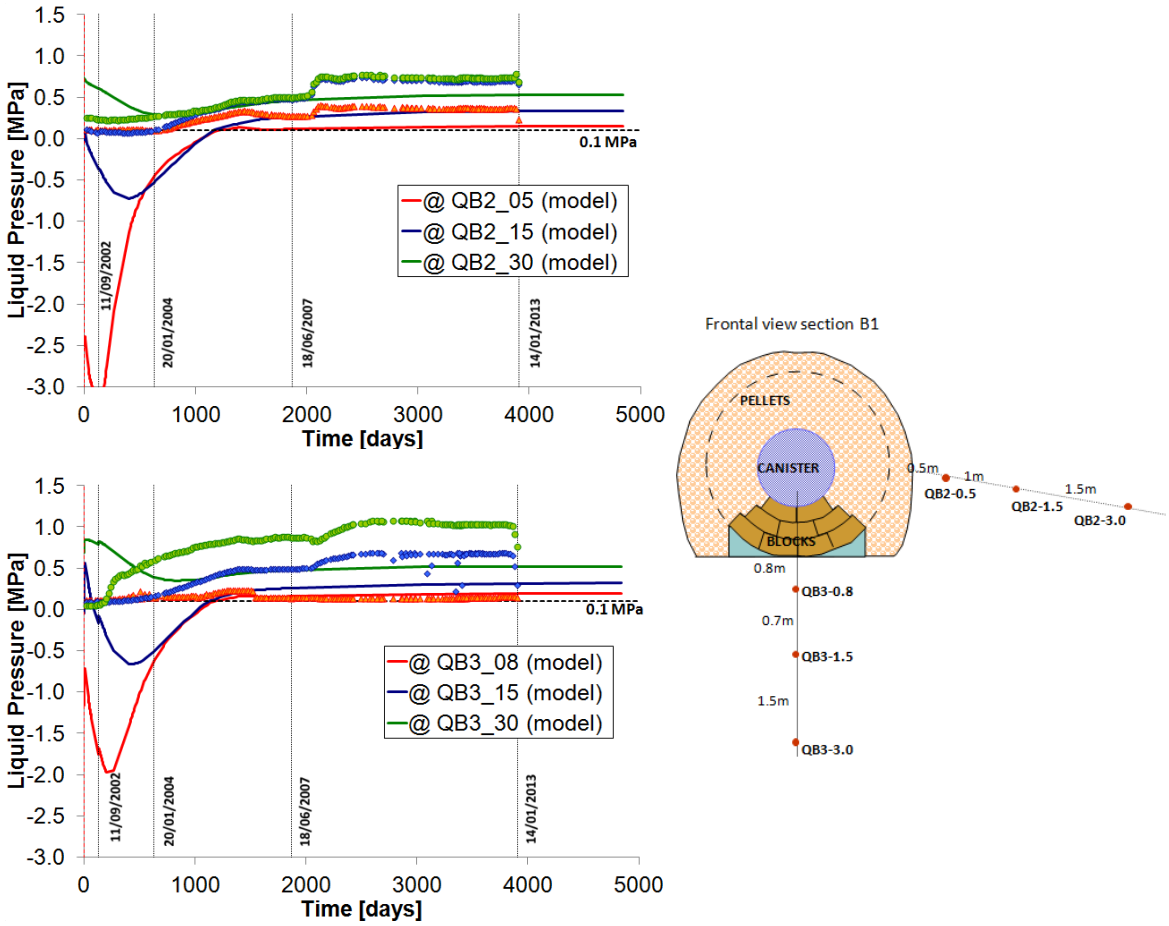

Figure19. Evolution of pore water pressure in the near field of the "EB" experiment. Model computations (full lines) and measured data (symbols) obtained from sensors in section B1

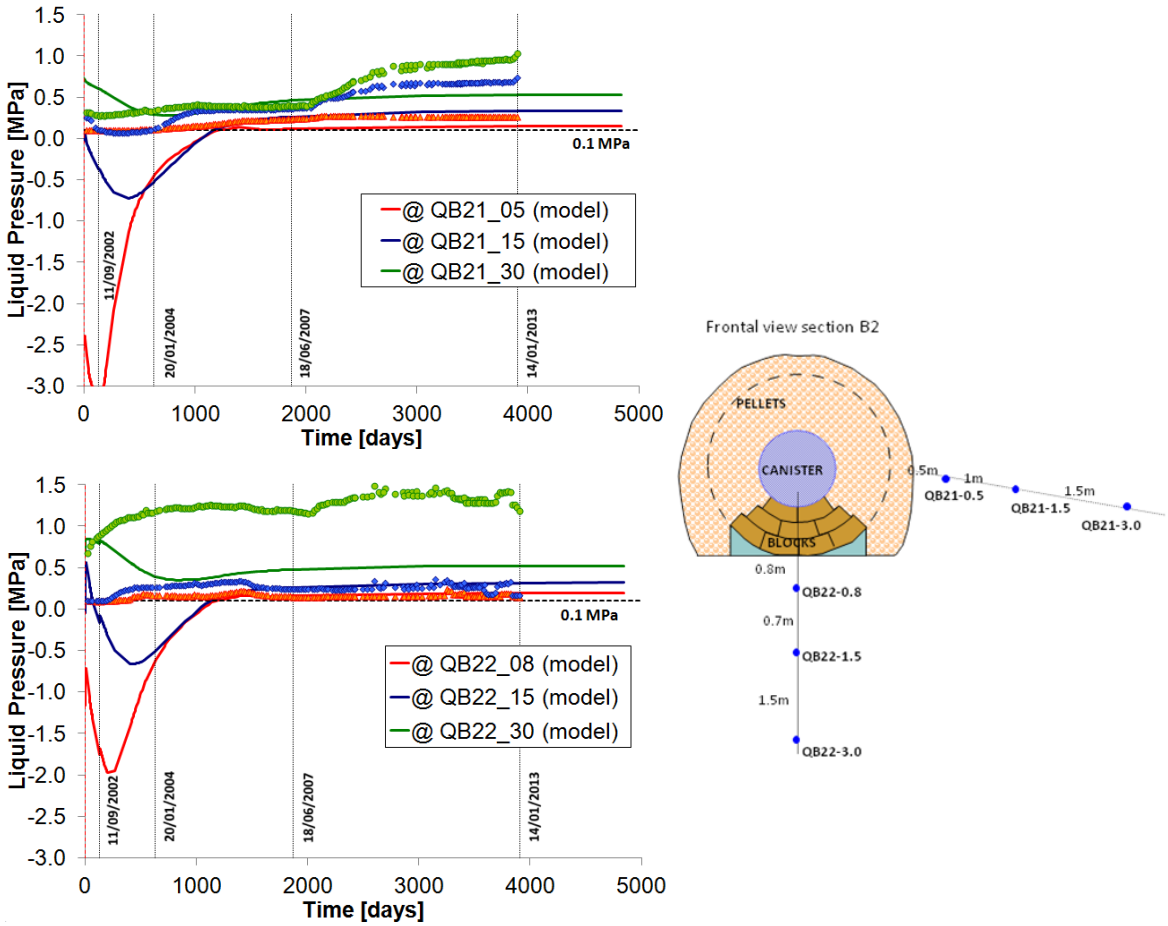

Figure 20. Evolution of pore water pressure in the near field of the "EB" experiment. Model computations (full lines) and measured data (symbols) obtained from sensors in section B2

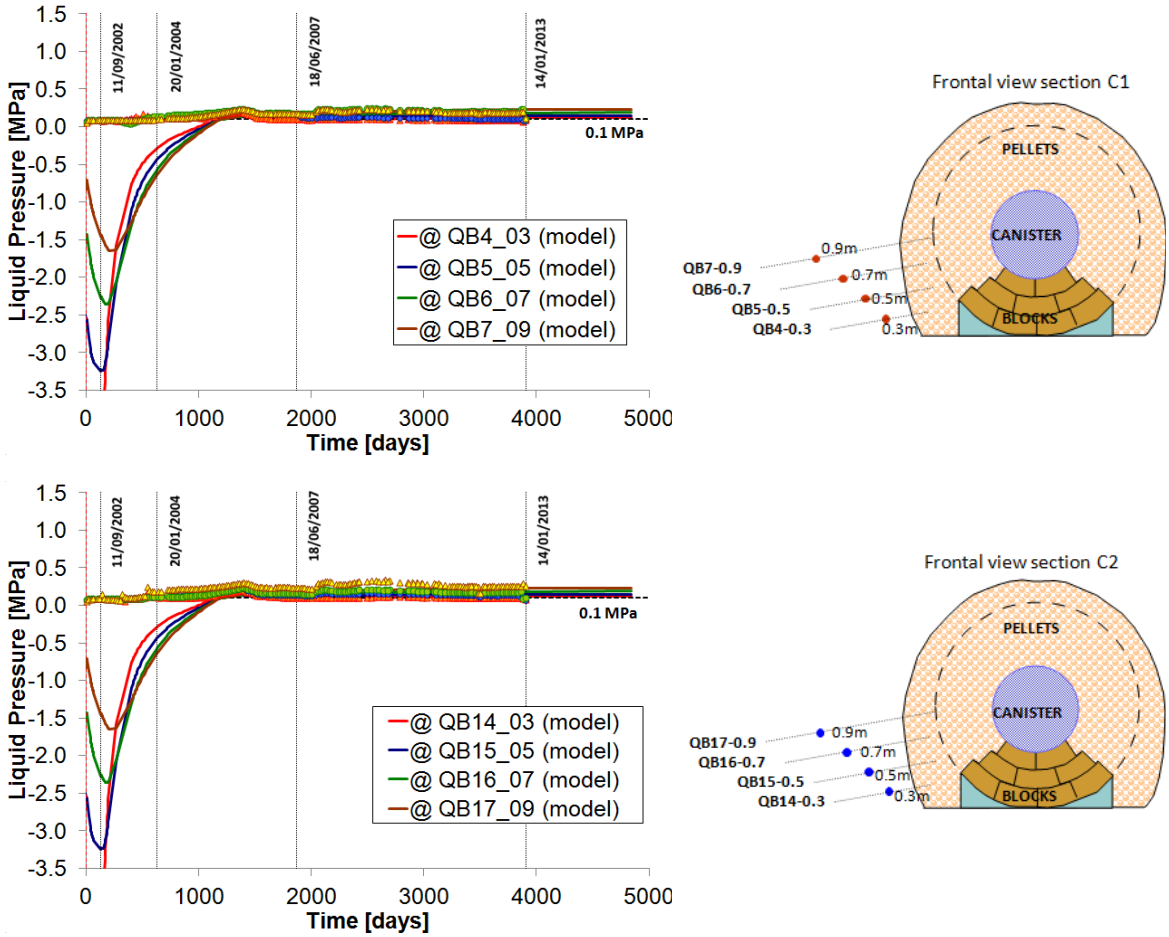

Figure 21. Evolution of pore water pressure in the host rock. Model computations (full lines) and measured data (symbols) obtained from sensors located in section C1 (up) and C2 (down)

5.3 Displacements of the cylinder

In order to measure the movement of the cylinder, two extensometers were installed in sections A1 and A2, located at its two ends. Measured and computed data are shown in Figure 22. In section A1 (sensors EA11 and EA12) an upward displacement of around 10 mm and a left to right horizontal displacement of 6 mm were recorded prior to the dismantling of the experiment while in section A2 (sensors EA21 and EA22) a maximum upward displacement of 8 mm and a maximum right to left displacement of about 17 mm were measured. The model naturally predicts a zero horizontal displacement (due to the symmetry conditions of the modelling) and an increment of upward movement close to 11 mm in the period comprised between the end of the first phase of hydration and the start of dismantling The vertical movement of the cylinder is due to the higher swelling capacity of the bentonite blocks compared with that of the granular bentonite.

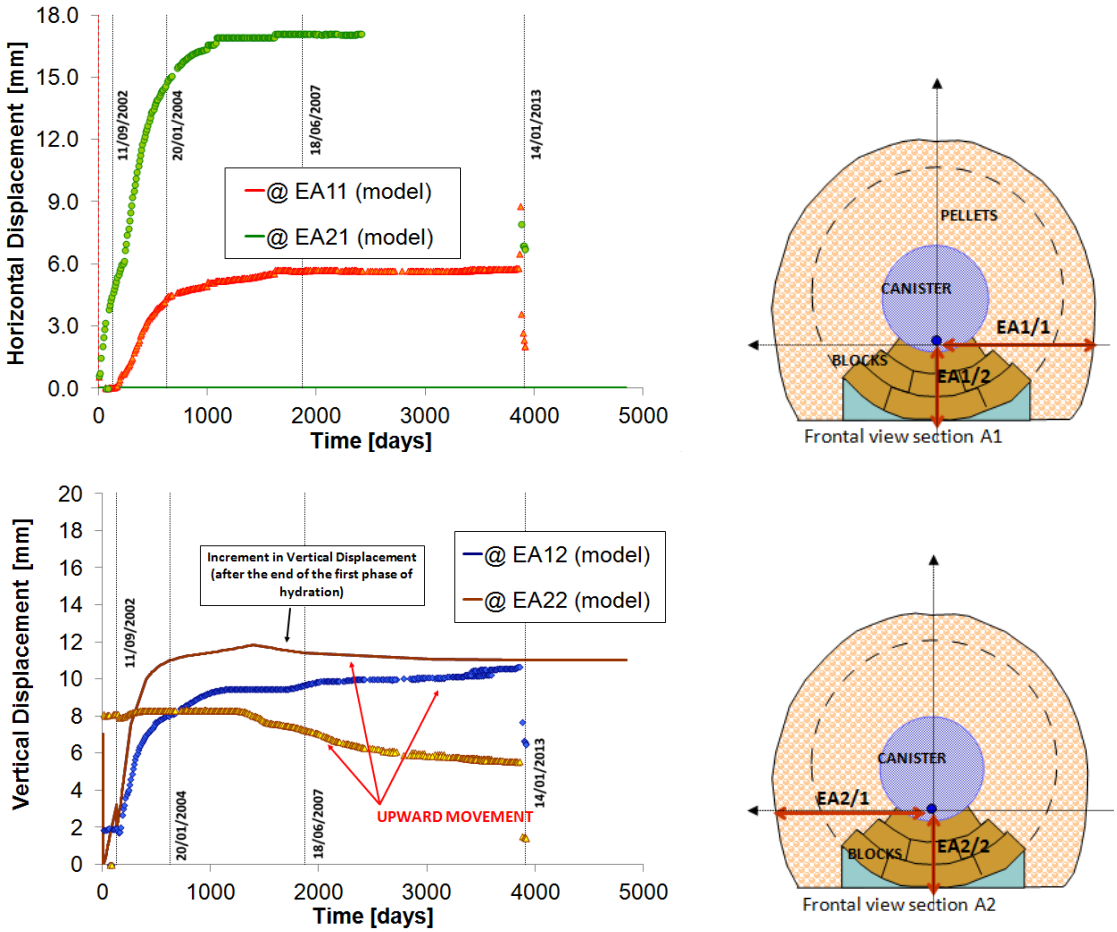

Figure 22. Measured and computed horizontal (up) and vertical (down) movement of the cylinder during the EB experiment. Calculated vertical displacement is referred to the end of the first phase of hydration. A positive measurement in the vertical direction indicates an upward movement and a positive measurement in the horizontal direction is interpreted as a left side movement of the cylinder from a frontal view

6. RESULTS FROM DISMANTLING

To characterize the final state of the barrier of the tests, numerous samples were taken during dismantling and tested in situ to determine their water content and their density. From that data, the corresponding degrees of saturation can be determined. Sampling and testing operations as well as the results obtained have been presented in Deliverable 2.1-4 (AITEMIN 2013).

Predicted spatial distributions of the degree of saturation inside the clay barrier along some radial profiles are plotted in Figure 23 together with the measured data from specimens recovered in the various sampling sections. The locations of the various profiles are indicated in the cross sections included in the Figure. Note that distances are referred to the steel cylinder surface. Both measured and computed values indicate an almost full saturation of the barrier when dismantling took place. In Figure 23, contours of computed degrees of saturation are also shown; as all computed values are above 98.5%, the information conveyed is not significant.

More relevant are the results concerning the distributions of dry density. Figures 24 and 25 show the comparison of computed dry density distributions and experimental data along several profiles of sampling sections A1-25 and E, respectively (see Figure 9 for the location of the sampling sections). The modelling results are in quite reasonable agreement with observations. Figures 26 and 27 illustrate the comparison of computed and experimental results in terms of computed contours of porosity and contours of dry density from experimental observations. Note that, for saturated samples, porosity and dry density are directly related by:

$$\rho_{dry} = \rho_s (1 - \phi) \tag{34}$$

where ρ_{dry} is the dry density, ρ_s the density of the solid phase and ϕ the porosity.

From Figures 24 to 27, it can be remarked that the bentonite barrier has undergone a large degree of homogenization. Considering vertical sections, especially, there is a great deal of homogenizations between blocks and granular bentonite. On occasion, the end dry density of the granular bentonite is even a little higher than that of the blocks (see sectionA1-25, for instance). This tendency is qualitatively well reproduced by the model as shown in Figures 22 to 25. It can also be observed that the lowest densities are measured in the lateral parts of the barrier especially in the lower zones. This observation is also satisfactorily reproduced by the numerical simulation.

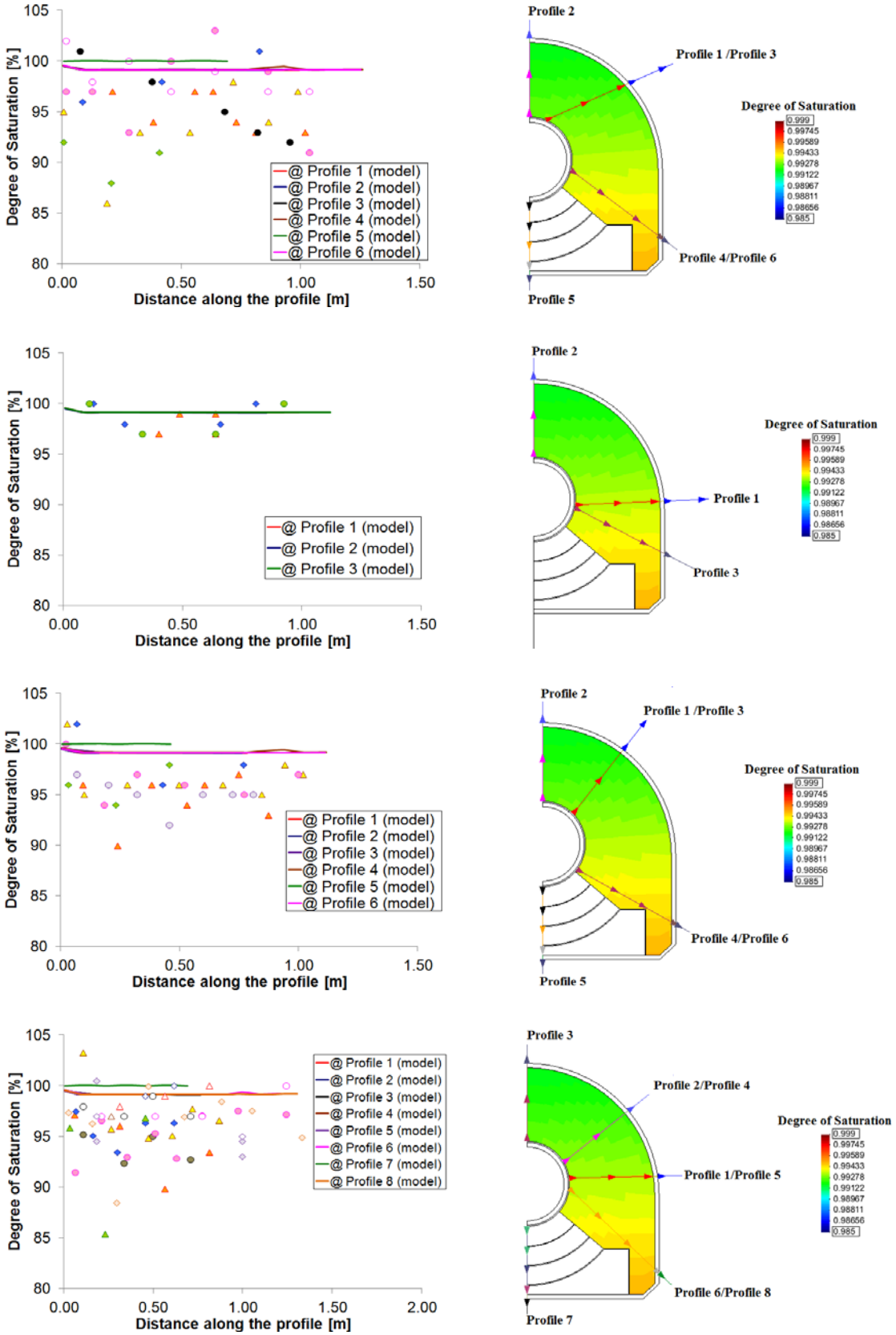

Figure 23. Computed distribution of degree of saturation along radial profiles located in several sampling sections (from top to bottom: A1-25, CMT-1, B1, E) measured at dismantling compared with experimental measurements (represented by symbols). Contours of degree of saturation are shown in the right column of the Figure

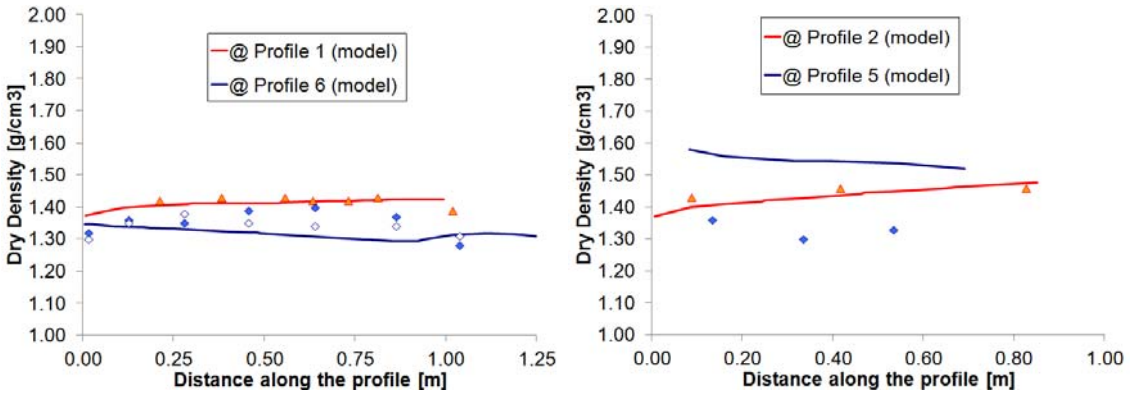

Figure 24. Computed distributions of dry density and experimental observations in section A1-25. The locations of the profiles are shown in Figure 26

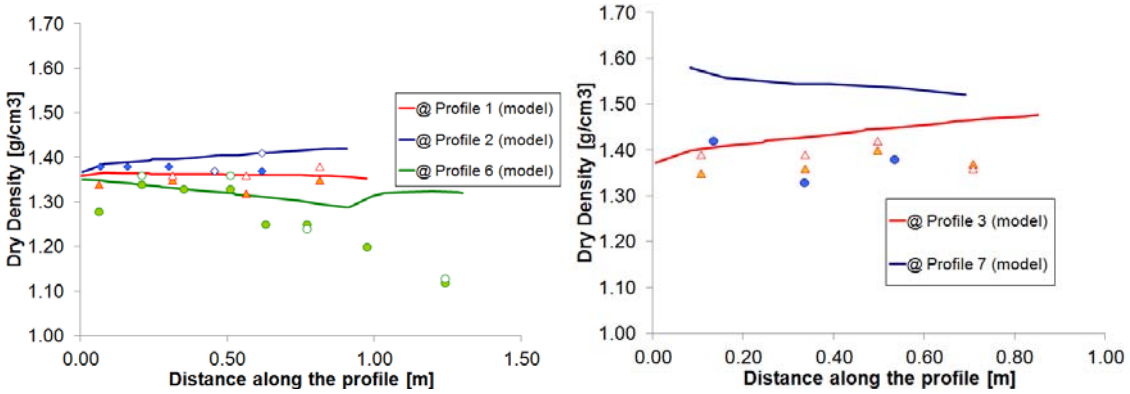

Figure 25. Computed distributions of dry density and experimental observations in section E. The locations of the profiles are shown in Figure 27

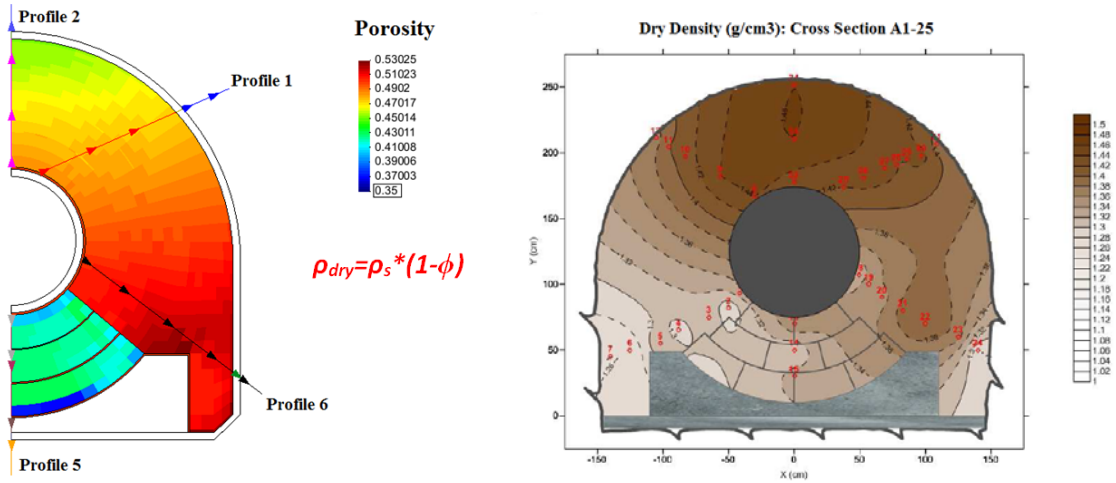

a) b)

Figure 26. Section A1-25. a) Computed contours of degree of saturation. b) Contours of dry density from dismantling data

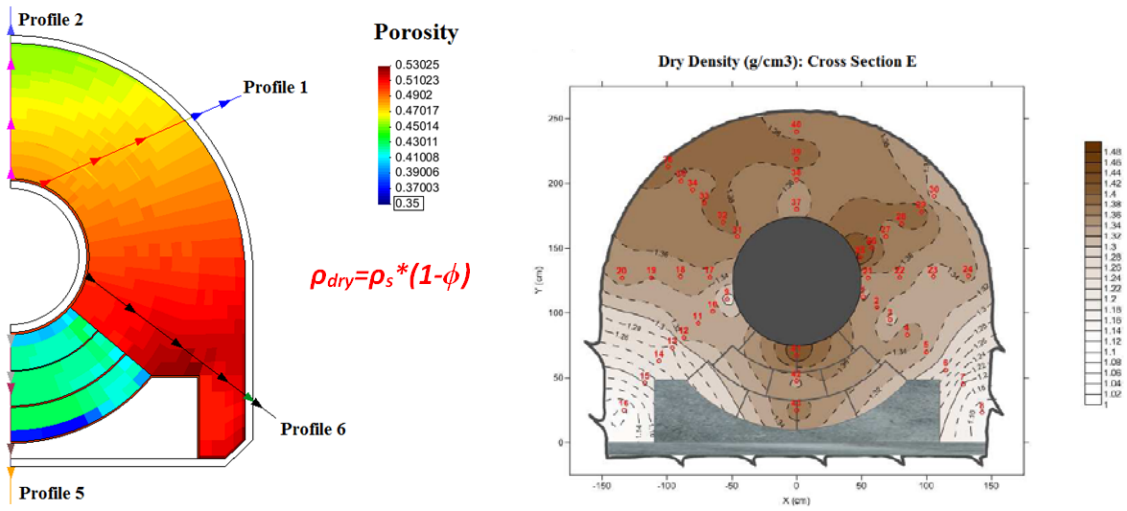

Figure 27. Section E. a) Computed contours of degree of saturation. b) Contours of dry density from dismantling data

7. SUMMARY AND CONCLUSIONS

In this report, the main activities related to the coupled HM analysis performed in relation to the EB experiment have been reported. The EB experiment is a demonstration test performed to prove the feasibility of constructing an engineered barrier using granular bentonite as the main buffer material. The test has been dismantled in the framework of the PEBS project after more than 10 years of operation. The test therefore provides an excellent case for assessing the evolution and state of the barrier after a relatively long period of time. Test interpretation is aided by the performance of suitable numerical simulations of the experiment.

The EB test has been performed under isothermal conditions; hence a coupled hydromechanical (HM) formulation is appropriate for analysing the problem. Because of the special characteristics of the granular bentonite employed as the main buffer material, a double porosity constitutive model that allows the consideration of two structural levels (macro and micro) has been adopted for its characterization.

The progress of hydration, as observed in the evolution of relative humidity (in the buffer and in the rock) and pore pressures (in the rock), is generally satisfactorily reproduced by the numerical model. The larger discrepancies concern the time evolution of relative humidity in the buffer. This is a likely consequence of the complexity of the artificial hydration system as well as the lack of control in some of the early hydration stages.

Dismantling has revealed two important facts: i) the barrier was at or very close to full saturation throughout, and ii) a significant degree of homogenization has been achieved although some heterogeneities persist even when the buffer has become (almost) fully saturated. It should be noted that the emplacement of the granular bentonite was affected by the presence of the hydration tubes and, to a lesser extent, sensors; so the observed heterogeneity may not be fully representative of that of an actual barrier.

The numerical model has also achieved a very good representation of the state of the barrier at dismantling. A practically fully saturated barrier is predicted and the degree of homogenization is also well reproduced in the simulation. Even the pattern of heterogeneity in the cross section of the barrier is satisfactorily simulated.

It has been considered likely that part of the heterogeneity observed upon dismantling may be caused by an initially heterogeneous barrier due to emplacement difficulties and likely segregation of the granular bentonite. It should be noted, however, that the numerical analyses have assumed an initially homogeneous granular bentonite. Therefore, the numerical modelling suggests that at least some of the observed heterogeneity at the dismantling stage is a direct consequence of the layout and geometry of the test.

Once more, it has been found that a properly formulated theoretical model together with appropriate constitutive laws and material parameters are capable of reproducing experimental observations in rather complex situations and over considerable periods of time. Thus, the availability of such proven numerical tools is a key ingredient in the achievement of a proper interpretation of experimental results and provides the means of making realistic predictions for the future behaviour of engineered barriers.

ACKNOWLEDGMENT

The research leading to results presented in this report has received funding from the European Atomic Energy Community's Seventh Framework Programme (FP/7 2007-2011) under grant agreement 249681.

REFERENCES

AITEMIN (2013) Engineered Barrier Emplacement Experiment in Opalinus Clay: "EB" Experiment. As-built of dismantling operation. Deliverable nº: D2.1-4. PEBS Project.

Alonso, E.E., Gens, A., Josa, A. (1990) A constitutive model for partially saturated soils. *Géotechnique*, 40, 405-430.

Alonso, E.E., Vaunat, J., Gens, A. (1999) Modelling the mechanical behaviour of expansive clays. *Engineering Geology,* 54, 173-183.

Alonso, E.E., Hoffman, C. (2007) Modelling the field behaviour of a granular expansive barrier. *Physics and Chemistry of the Earth,* 32, 850-865.

CODE_BRIGHT User's Manual (2014). UPC Geomechanical Group.

ENRESA (2000) FEBEX Project. Full scale engineered barriers experiment for a deep geological repository for high level radioactive waste in crystalline host rock. Final Report. Madrid, Spain.

Gens, A., Alonso, E.E. (1992) A framework for the behaviour of unsaturated expansive clays. *Canadian Geotechnical Journal,* 29, 1013-1032.

Gens, A., Garcia Molina, A, Olivella, S., Alonso, E.E. & Huertas, F. (1998). "Analysis of a full scale in-situ test simulating repository conditions". *Int. Jnl. Numer. Anal. Meth. Geomech*, 22, 515- 548.

Gens, A., Sánchez, M. (2014), Formulation of a model suitable for long term predictions. Deliverable D3.5-2. PEBS project

HE-E experiment (2013). Modellers as-built dataset for the model calibration. Version 3.

Hoffman, C. (2005) Caracterización hidromecánica de mezclas de pellets de bentonita. Estudio experimental y constitutivo. Doctoral Thesis, Technical University of Catalonia (UPC), Barcelona, Spain.

Hoffman, C., Alonso, E.E., Romero, E. (2007) Hydro-mechanical behaviour of bentonite pellet mixtures. *Physics and Chemistry of the Earth*, 32, 832-849.

Mayor, J.C., García-Siñériz, J.L., Alonso, E., Alheid, H.J., Blümbling, P. (2005). Engineered barrier emplacement experiment in Opalinus Clay for the disposal of radioactive waste in underground repositories. Final Technical Publishable Report.

Olivella, S., Gens, A., Carrera, J. & Alonso, E.E. (1996). "Numerical formulation for a simulator (CODE-BRIGHT) for the coupled analysis of saline media". *Engineering Computations*, 13, 87-112.

Sánchez, M., Gens, A., Guimaraes, L. do N., Olivella, S. (2005) A double structure generalized plasticity model for expansive materials. *International Journal for Numerical and Analytical Methods in Geomechanics,* 29, 751-787.

van Genuchten, R. (1978). "Calculating the unsaturated hydraulic permeability conductivity with a new closed-form analytical model". *Water Resource Research*. 37, 21-28